Excerpt from Chapter 13 of :

Legendre, P. and L. Legendre. 2012. Numerical ecology, 3rd English edition. Elsevier Science BV, Amsterdam. xvi + 990 pp.

13.1 Structure functions

Ecologists are interested in describing spatial structures in quantitative ways and testing for the presence of spatial correlation in data. The primary objective is to:

- either support the null hypothesis that no significant spatial correlation is present in a data set, or that none remains after detrending (Subsection 13.2.1) or after controlling for the effect of explanatory (e.g. environmental) variables, thus insuring valid use of the standard univariate or multivariate statistical tests of hypotheses,

- or reject the null hypothesis and show that significant spatial correlation is present in the data, in order to use it in conceptual or statistical models.

Tests of spatial correlation coefficients may only support or reject the null hypothesis of the absence of significant spatial structure. When a significant spatial structure is found, it may correspond to induced spatial dependence (Subsection 1.1.1, model 1) or true spatial autocorrelation (model 2).

Map

Spatial structures may be described through *structure functions*, which allow one to quantify the spatial dependence and partition it amongst distance classes. Interpretation of that description is usually supported by maps of the univariate or multivariate data (Sections 13.2 to 13.4). The most commonly used spatial structure functions are correlograms, variograms, and periodograms.

Spatial correlogram

A *correlogram* is a graph in which spatial correlation values are plotted, on the ordinate, against *distance classes* among sites on the abscissa. Correlograms (Cliff & Ord, 1981) can be computed for single variables (Moran's I or Geary's c, Subsection 13.1.1, or the spatial correlation function, Subsection 13.1.5) or for multivariate data (multivariate variogram, Subsection 13.1.4, and Mantel correlogram, Subsection 13.1.6). In all cases, a test of significance is available for each individual spatial correlation coefficient plotted in a correlogram.

Variogram

Similarly, a *variogram* is a graph in which semi-variance is plotted, on the ordinate, against *distance classes* among sites on the abscissa (Subsection 13.1.3). In the geostatistical tradition, semi-variance statistics are not tested for significance, although they could be through the test developed for Geary's c, when the condition of second-order stationarity is satisfied (Subsection 13.1.1). Statistical models may be fitted to variograms (linear, exponential, spherical, Gaussian, etc.); they allow the investigator to relate the observed structure to hypothesized generating processes or to produce interpolated maps by kriging (Subsection 13.2.2).

Because they measure the relationship between pairs of observation points located a certain distance apart, correlograms and variograms may be computed either for preferred geographic directions or, when the phenomenon is assumed to be isotropic in space, in an all-directional way.

2-D periodogram

A *two-dimensional Schuster* (1898) *periodogram* may be computed when the structure under study is assumed to consist of a combination of sine waves propagated through space. The basic idea is to fit sines and cosines of various periods, one period at a time, and to determine the proportion of the series' variance (r^2) explained by each period. In periodograms, the abscissa is either a period or its inverse, a frequency; the ordinate is the proportion of variance explained. Two-dimensional periodograms may be plotted for all combinations of directions and spatial frequencies. The technique is applicable to regular grids of points; it is described Priestley (1964), Ripley (1981), Renshaw and Ford (1984) and Legendre & Fortin (1989). It is not discussed further in this book. Spatial eigenfunction analysis, described in Chapter 14, carries out a similar form of analysis and is more general since it can be used on irregularly-spaced points.

1 — Spatial correlograms

For quantitative variables (univariate data), spatial correlation can be estimated by Moran's *I* (1950) or Geary's *c* (1954) spatial correlation statistics[*] (Cliff & Ord, 1981):

Moran's *I*:
$$I(d) = \frac{\frac{1}{W}\sum_{h=1}^{n}\sum_{i=1}^{n} w_{hi}(y_h-\bar{y})(y_i-\bar{y})}{\frac{1}{n}\sum_{i=1}^{n}(y_i-\bar{y})^2} \quad \text{for } h \neq i \qquad \textbf{(13.1)}$$

Geary's *c*:
$$c(d) = \frac{\frac{1}{2W}\sum_{h=1}^{n}\sum_{i=1}^{n} w_{hi}(y_h-y_i)^2}{\frac{1}{(n-1)}\sum_{i=1}^{n}(y_i-\bar{y})^2} \quad \text{for } h \neq i \qquad \textbf{(13.2)}$$

y_h and y_i are the values of the observed variable at sites *h* and *i*, and *d* is the distance class considered in the calculation. Before computing spatial correlation coefficients, a matrix of geographic distances $\mathbf{D} = [D_{hi}]$ among observation sites must be calculated. Statistical details about these coefficients are available in Cliff & Ord (1981) and d'Aubigny (2006).

In the presence of explanatory variables generating spatial structure in the variable of interest, true spatial autocorrelation must be estimated on the *residuals* of a model that takes these explanatory variables into account. This is in agreement with the definition of spatial autocorrelation (Section 1.1), which is the spatial dependence *among the error components* of the observed data (eq. 1.2).

[*] These statistics are often called spatial *autocorrelation* coefficients. This terminology is misleading since the coefficients measure any type of spatial structure, be it due to induced spatial dependence (eq. 1.1) or true spatial autocorrelation (eq. 1.2).

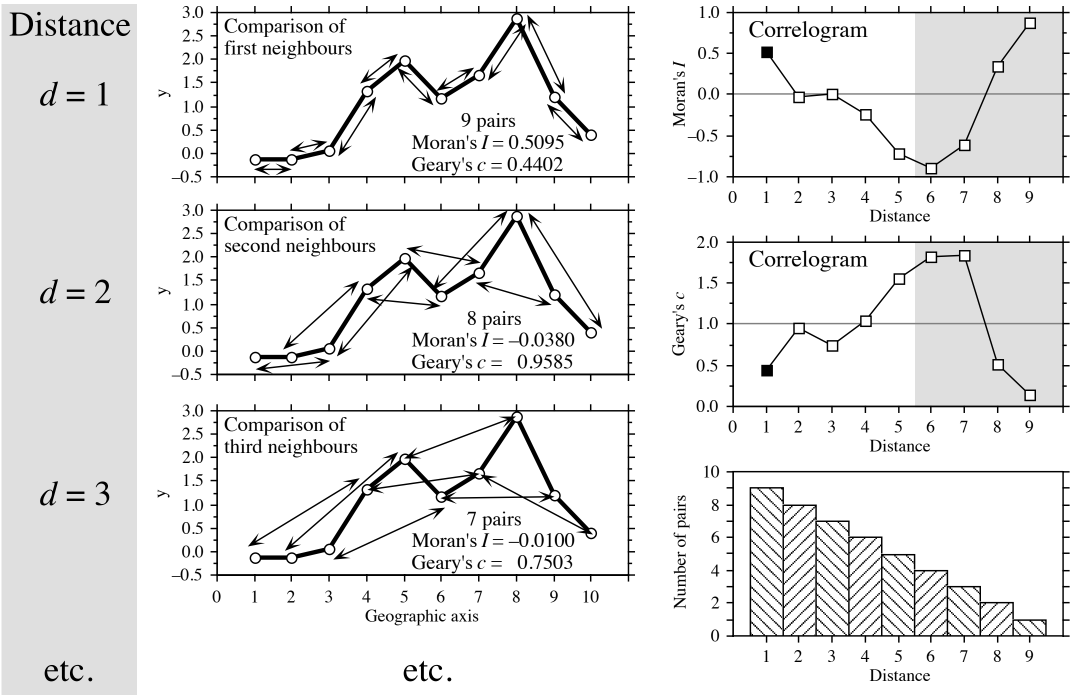

Figure 13.3 Construction of correlograms. Left: data series observed along a single geographic axis (10 equispaced observations). Moran's I and Geary's c statistics are computed from pairs of observations found at preselected distances ($d = 1$, $d = 2$, $d = 3$, etc.). Right: correlograms are graphs of the spatial correlation statistics plotted against distance. Dark squares: significant correlation statistics ($p \leq 0.05$). Lower right: histogram showing the number of pairs in each distance class. Coefficients for the larger distance values (grey zones in correlograms) should not be considered in correlograms, nor interpreted, because they are based on a small number of pairs (test with low power) and exclude some points found in the centre of the series or surface.

In the construction of a correlogram, spatial correlation coefficients are computed, in turn, for the various distance classes d. The weights w_{hi} are Kronecker deltas (as in eq. 7.21); the binary weights take the value $w_{hi} = 1$ when sites h and i are at distance d and $w_{hi} = 0$ otherwise. In this way, only the pairs of sites (h, i) within the stated distance class (d) are taken into account in the calculation of any given coefficient. This approach is illustrated in Fig. 13.3. W is the sum of the weights w_{hi} for the given distance class, i.e. the number of pairs used to calculate the coefficient. For a given distance class, the weights w_{ij} are written in a ($n \times n$) spatial weighting matrix $\mathbf{W}$; an example of a binary spatial weighting matrix is matrix $\mathbf{X}(1)$ of Fig. 13.14. Jumars *et al.* (1977) present ecological examples where the distance^{-1} or distance^{-2} among adjacent sites is used for weight instead of 1's.

The numerators of eqs. 13.1 and 13.2 are written with summations involving each pair of objects twice; in eq. 13.2 for example, the terms $(y_h - y_i)^2$ and $(y_i - y_h)^2$ are both used in the summation. This allows for cases where the distance matrix **D** or the weight matrix **W** is asymmetric. In studies of the dispersion of pollutants in soil, for instance, drainage may make it more difficult to go from A to B than from B to A; this may be recorded as a larger distance from A to B than from B to A. In spatio-temporal analyses, an observed value may influence a later value at the same or a different site, but not the reverse. An impossible connection may be coded by a very large value of distance or by $w_{hi} = 0$. In most applications, however, the geographic distance matrix among sites is symmetric and the coefficients can be computed from the half-matrix of distances; the formulae remain the same, because W and the sum in the numerator are half the values computed over the whole distance matrix **D**.

One may use distances along a network of connections (Subsection 13.3.1) instead of straight-line geographic distances; this includes the "chess moves" for regularly-spaced points as obtained from systematic sampling designs: rook's, bishop's, or king's connections (see Fig. 13.21). For very broad-scale studies, involving a whole ocean or continent, "great-circle distances", i.e. distances along the earth's curved surface, should be used instead of straight-line distances through the earth crust.

Moran's I formula is related to the Pearson correlation coefficient; its numerator is a covariance, comparing the values found at all pairs of points in turn, while its denominator is the maximum-likelihood estimator of the variance (i.e. division by n instead of $n - 1$); in Pearson r, the denominator is the product of the standard deviations of the two variables (eq. 4.7), whereas in Moran's I there is only one variable involved. Moran's I mainly differs from Pearson r in that the sums in the numerator and denominator of eq. 13.1 do not involve the same number of terms; only the terms corresponding to distances within the given class are considered in the numerator whereas all pairs are taken into account in the denominator. Moran's I usually takes values in the interval $[-1, +1]$ although values lower than -1 or higher than $+1$ may occasionally be obtained. Positive spatial correlation in the data translates into positive values of I; negative correlation produces negative values.

Readers who are familiar with correlograms in time series analysis (Section 12.3) will be reassured to know that, when a problem involves equispaced observations along a single physical dimension, as in Fig. 13.3, calculating Moran's I (eq. 13.1) for the different distance classes is nearly the same as computing the autocorrelation coefficient of time series analysis (Fig. 12.5, eq. 12.7).

Geary's c coefficient is a distance-type function; it varies from 0 to some unspecified value larger than 1. Its numerator sums the squared differences between values found at the various pairs of sites being compared. A Geary's c correlogram varies as the reverse of a Moran's I correlogram; strong spatial correlation produces high values of I and low values of c (Fig. 13.3). Positive spatial correlation translates in values of c between 0 and 1 whereas negative correlation produces values larger than 1. Hence, the reference 'no correlation' value is $c = 1$ in Geary's correlograms.

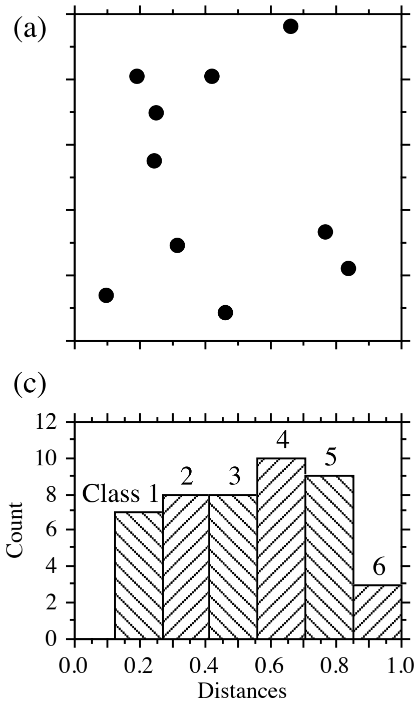

(b)

$$\mathbf{D} = \begin{bmatrix} 0.00 & 0.52 & 0.74 & 0.20 & 0.31 & 0.29 & 0.72 & 0.72 & 0.59 & 0.23 \\ 0.52 & 0.00 & 0.27 & 0.41 & 0.27 & 0.75 & 0.52 & 0.25 & 0.45 & 0.53 \\ 0.74 & 0.27 & 0.00 & 0.58 & 0.44 & 1.00 & 0.74 & 0.37 & 0.70 & 0.67 \\ 0.20 & 0.41 & 0.58 & 0.00 & 0.15 & 0.49 & 0.76 & 0.65 & 0.63 & 0.12 \\ 0.31 & 0.27 & 0.44 & 0.15 & 0.00 & 0.59 & 0.68 & 0.51 & 0.57 & 0.26 \\ 0.29 & 0.75 & 1.00 & 0.49 & 0.59 & 0.00 & 0.76 & 0.90 & 0.64 & 0.50 \\ 0.72 & 0.52 & 0.74 & 0.76 & 0.68 & 0.76 & 0.00 & 0.40 & 0.13 & 0.87 \\ 0.72 & 0.25 & 0.37 & 0.65 & 0.51 & 0.90 & 0.40 & 0.00 & 0.39 & 0.77 \\ 0.59 & 0.45 & 0.70 & 0.63 & 0.57 & 0.64 & 0.13 & 0.39 & 0.00 & 0.74 \\ 0.23 & 0.53 & 0.67 & 0.12 & 0.26 & 0.50 & 0.87 & 0.77 & 0.74 & 0.00 \end{bmatrix}$$

(d)

$$\mathbf{D} = \begin{bmatrix} — & & & & & & & & & \\ 3 & — & & & & & & & & \\ 5 & 2 & — & & & & & & & \\ 1 & 2 & 4 & — & & & & & & \\ 2 & 2 & 3 & 1 & — & & & & & \\ 2 & 5 & 6 & 3 & 4 & — & & & & \\ 5 & 3 & 5 & 5 & 4 & 5 & — & & & \\ 5 & 1 & 2 & 4 & 3 & 6 & 2 & — & & \\ 4 & 3 & 4 & 4 & 4 & 4 & 1 & 2 & — & \\ 1 & 3 & 4 & 1 & 1 & 3 & 6 & 5 & 5 & — \end{bmatrix}$$

Figure 13.4 Calculation of distance classes, artificial data. (a) Map of 10 sites in a 1-km^2 sampling area. (b) Geographic distance matrix (**D**, in km). (c) Frequency histogram of distances (classes 1 to 6) for the upper (or lower) triangular portion of **D**. (d) Distances recoded into 6 classes.

For sites lying on a surface or in a volume, geographic distances do not naturally fall into a small number of values; this is true for regular grids as well as random or other forms of irregular sampling designs. Distance values must be grouped into distance classes; in this way, each spatial correlation coefficient can be computed using several comparisons of sampling sites.

Numerical example. In Fig. 13.4 (artificial data), 10 sites have been located at random into a 1-km^2 sampling area. Euclidean (geographic) distances were computed among sites. The number of classes is arbitrary and left to the user's decision. A compromise has to be made between resolution of the correlogram (more resolution when there are more, narrower classes) and power of the test (more power when there are more pairs in a distance class). Sturges' (1926) rule is often used to decide about the number of classes in histograms; it was used here and gave:

$$\text{Number of classes} = 1 + 3.322\log_{10}(m) = 1 + 3.3\log_{10}(45) = 6.46 \qquad \textbf{(13.3)}$$

where m is the number of distances in the upper triangular matrix and 3.322 is $1/\log_{10}2$; the number was rounded to the nearest integer (i.e. 6). The distance matrix was thus recoded into 6 classes, ascribing class numbers (1 to 6) to all distances within a class of the histogram.

An alternative to distance classes with equal widths would be to create distance classes containing the same number of pairs (notwithstanding tied values); distance classes formed in this way are of unequal widths. The advantage is that the tests of significance have the same power across all distance classes because they are based upon the same number of pairs of observations. The disadvantages are that limits of the distance classes are more difficult to find and correlograms are harder to draw.

Spatial correlation coefficients can be tested for significance and confidence intervals can be computed. With proper correction for multiple testing, one can determine if a significant spatial structure is present in the data and what are the distance classes showing significant positive or negative correlation. Tests of significance require, however, that certain conditions specified below be fulfilled.

Second-order stationarity

The tests require that the condition of *second-order stationarity* be satisfied. Second-order stationarity refers to the vectors separating pairs of values in the study area. This rather strong condition states that the mean of the variable is constant over the study area, and the spatial covariance (numerator of eq. 13.1) depends only on the length and orientation of the vector between any two points, not on its position in the study area (David, 1977). The variance (denominator of eq. 13.1) must be the same for all points in the study area (homogeneity of the variance; Dutilleul, 2011).

Intrinsic stationarity

A relaxed form of stationarity, called *intrinsic stationarity*, states that the differences $(y_h - y_i)$ for any distance d (numerator of eq. 13.2) must have zero mean and constant and finite variance over the study area, independently of the location where the differences are calculated. Here, one considers the *increments* of the values of the regionalized variable instead of the values themselves (David, 1977). As shown below, the variance of the increments is the variogram function. In layman's terms, this means that a single spatial correlation function is adequate to describe the entire surface under study. An example where intrinsic stationarity does not hold is a region which is half plain and half mountains; such a region should be divided in two subregions in which the variable "altitude" could be modelled by separate spatial correlation functions. Second-order stationarity implies intrinsic stationarity, but the reciprocal is not true. Intrinsic stationarity is a weaker form of stationarity compatible with a broader range of models. This condition must always be met when variograms or correlograms (including multivariate Mantel correlograms) are computed, even for descriptive purpose.

Cliff & Ord (1981) describe how to compute confidence intervals and test the significance of spatial correlation coefficients. For any normally distributed statistic *Stat*, a confidence interval at significance level α is obtained as follows:

$$Pr\left(Stat - z_{\alpha/2}\sqrt{\mathrm{Var}(Stat)} < Stat_{\mathrm{Pop}} < Stat + z_{\alpha/2}\sqrt{\mathrm{Var}(Stat)}\right) = 1 - \alpha \qquad \mathbf{(13.4)}$$

For significance testing with large samples, a one-tailed critical value $Stat_\alpha$ at significance level α is obtained as follows:

$$Stat_\alpha = z_\alpha \sqrt{\mathrm{Var}\,(Stat)} + \text{Expected value of } Stat \text{ under } \mathrm{H}_0 \qquad \textbf{(13.5)}$$

It is possible to use this approach because both I and c are asymptotically normally distributed for data sets of moderate to large sizes (Cliff & Ord, 1981). Values $z_{\alpha/2}$ or z_α are found in a table of standard normal deviates. Under the hypothesis (H_0) of random spatial distribution of the observed values y_i, the expected values (E) of Moran's I and Geary's c are:

$$E(I) = -(n-1)^{-1} \quad \text{and} \quad E(c) = 1 \qquad \textbf{(13.6)}$$

Under the null hypothesis, the expected value of Moran's I approaches 0 as n increases. The variances are computed as follows under a randomization assumption, which simply states that, under H_0, the observations y_i are independent of their positions in space (second-order stationarity assumption) and, thus, are exchangeable:

$$\mathrm{Var}\,(I) = \mathrm{E}\,(I^2) - [\mathrm{E}\,(I)]^2 \qquad \textbf{(13.7)}$$

$$\mathrm{Var}\,(I) = \frac{n[(n^2-3n+3)S_1 - nS_2 + 3W^2] - b_2[(n^2-n)S_1 - 2nS_2 + 6W^2]}{(n-1)(n-2)(n-3)W^2} - \frac{1}{(n-1)^2}$$

$$\mathrm{Var}\,(c) = \frac{(n-1)S_1[n^2-3n+3-(n-1)b_2]}{n(n-2)(n-3)W^2} \qquad \textbf{(13.8)}$$

$$+\ \frac{-0.25(n-1)S_2[n^2+3n-6-(n^2-n+2)b_2] + W^2[n^2-3+(-(n-1)^2)b_2]}{n(n-2)(n-3)W^2}$$

In these equations,

- $S_1 = \frac{1}{2}\sum_{h=1}^{n}\sum_{i=1}^{n}(w_{hi}+w_{ih})^2$ (there is a term of this sum for *each cell* of matrix **W**);
- $S_2 = \sum_{i=1}^{n}(w_{i+}+w_{+i})^2$ where w_{i+} and w_{+i} are respectively the sums of row i and column i of matrix **W**;
- $b_2 = n\sum_{i=1}^{n}(y_i-\bar{y})^4 \Big/ \left[\sum_{i=1}^{n}(y_i-\bar{y})^2\right]^2$ measures the kurtosis of the distribution;
- W is as defined in eqs. 13.1 and 13.2.

In most cases in ecology, tests of spatial correlation are one-tailed because the sign of the correlation is stated in the ecological hypothesis; for instance, contagious biological processes such as growth, reproduction, and dispersal, all suggest that ecological variables are positively correlated at short distances. To carry out an approximate test of significance, select a value of α (e.g. $\alpha = 0.05$) and find z_α in a table of the standard normal distribution (e.g. $z_{0.05} = +1.6452$). Critical values are found as in eq. 13.5, with a correction factor that becomes important when n is small:

- $I_\alpha = z_\alpha \sqrt{\mathrm{Var}(I)} - k_\alpha (n-1)^{-1}$ in all cases, using the value in the upper tail of the z distribution when testing for positive spatial correlation (e.g. $z_{0.05} = +1.6452$), and the value in the lower tail in the opposite case (e.g. $z_{0.05} = -1.6452$);

- $c_\alpha = z_\alpha \sqrt{\mathrm{Var}(c)} + 1$ when $c < 1$ (positive spatial correlation), using the value in the lower tail of the z distribution (e.g. $z_{0.05} = -1.6452$);

- $c_\alpha = z_\alpha \sqrt{\mathrm{Var}(c)} + 1 - k_\alpha (n-1)^{-1}$ when $c > 1$ (negative spatial correlation), using the value in the upper tail of the z distribution (e.g. $z_{0.05} = +1.6452$).

The value taken by the correction factor k_α depends on the values of n and W. If $4(n - \sqrt{n}) < W \le 4(2n - 3\sqrt{n} + 1)$, then $k_\alpha = \sqrt{10\alpha}$; otherwise, $k_\alpha = 1$. If the test is two-tailed, use $\alpha^* = \alpha/2$ to find z_{α^*} and k_{α^*} before computing critical values. These corrections are based upon simulations reported by Cliff & Ord (1981, Section 2.5).

Other formulas are found in Cliff & Ord (1981) for conducting a test under the assumption of normality, where one assumes that the y_i's result from n independent draws from a normal population. When n is very small, tests of I and c should be conducted by permutation (Subsection 1.2.2).

Moran's I and Geary's c are sensitive to extreme values and, in general, to asymmetry in the data distributions, as are the related Pearson r and Euclidean distance coefficients. Asymmetry increases the variance of the data. It also increases the kurtosis and hence the variance of the I and c coefficients (eqs. 13.7 and 13.8); this makes it more difficult to reach significance in statistical tests. So, practitioners usually attempt to normalize the data before computing correlograms and variograms.

Statistical testing in correlograms implies multiple testing since a test of significance is carried out for each spatial correlation coefficient. Oden (1984) has developed a Q statistic to test the global significance of spatial correlograms; his test is an extension of the Portmanteau Q-test used in time series analysis (Box & Jenkins, 1976). An alternative global test is to check whether the correlogram contains at least one correlation statistic that is significant at the Bonferroni-corrected significance level (Box 1.3). Simulations by Oden (1984) showed that the power of the Q-test is not appreciably greater than the power of the Bonferroni procedure, which is computationally a lot simpler. A practical question remains, though: how many distance classes should be created? This determines the number of simultaneous tests that are carried out. More classes mean more resolution but fewer pairs per class and, thus, less power for each test; more classes also mean a smaller Bonferroni-corrected α' level, which makes it more difficult for a correlogram to reach global significance.

When the overall test has shown global significance, one may wish to identify the individual spatial correlation statistics that are significant, in order to reach an interpretation (Subsection 13.1.2). One could rely on Bonferroni-corrected tests for all individual correlation statistics, but this approach would be too conservative; a better solution is to use Holm's correction procedure (Box 1.3). Another approach is the *progressive Bonferroni correction* described in Subsection 12.4.2; it is only applicable when the ecological hypothesis indicates that significant spatial correlation is to be expected in the smallest distance classes and the purpose of the analysis is to determine the extent of the spatial correlation (i.e. which distance class it reaches). With the progressive Bonferroni approach, the likelihood of emergence of significant values decreases as one proceeds from left to right, i.e. from the small to the large distance classes of the correlogram. In addition, one does not have to limit the correlogram to a small number of classes to reduce the effect of the correction, as it is the case with Oden's overall test and with the Bonferroni and Holm correction methods. This approach will be used in the examples that follow.

Spatial correlation coefficients and tests of significance also exist for qualitative (nominal) variables (Cliff & Ord, 1981); they have been used, for example, to analyse spatial patterns of sexes in plants (Sakai & Oden, 1983; Sokal & Thomson, 1987). Special types of spatial correlation coefficients have been developed to answer specific problems (e.g. Galiano, 1983; Estabrook & Gates, 1984). The paired-quadrat variance method, developed by Goodall (1974) to analyse spatial patterns of ecological data by random pairing of quadrats, is related to correlograms.

2 — Interpretation of all-directional correlograms

Isotropy
Anisotropy

When the spatial correlation function is the same for all geographic directions considered, the phenomenon is *isotropic*. The opposite of isotropy is *anisotropy.* When a variable is isotropic, a single correlogram can be computed over all directions of the study area. The correlogram is said to be *all-directional* or *omnidirectional*. Directional correlograms, which are computed for a single spatial direction, are discussed together with anisotropy and directional variograms in Subsection 13.1.3.

Correlograms are analysed mostly by looking at their shapes. Examples will help clarify the relationship between spatial structures and all-directional correlograms. The important message is that, although correlograms may give clues as to the underlying spatial structure, the information they provide is not specific; a blind interpretation may be misleading and should be supported by examination of maps (Section 13.2).

Numerical example. Artificial data were generated that correspond to a number of spatial patterns. The data and resulting correlograms are presented in Fig. 13.5.

1. Nine bumps. — The surface in Fig. 13.5a is made of nine bi-normal curves. 225 points were sampled across the surface using a regular 15 × 15 grid (Fig. 13.5f). The "height" was noted at each sampling point. The 25200 distances among points found in the upper-triangular portion of the distance matrix were divided into 16 distance classes, using Sturges' rule (eq. 13.3), and correlograms were computed. According to Oden's test, the correlograms were globally significant at the $\alpha = 5\%$ level since several individual values were significant at the Bonferroni-corrected level $\alpha' = 0.05/16 = 0.00312$. In each correlogram, the progressive Bonferroni correction method was applied to identify significant spatial correlation coefficients: the coefficient for distance class 1 was tested at the $\alpha = 0.05$ level; the coefficient for distance class 2 was tested at the $\alpha' = 0.05/2$ level; and, more generally, the coefficient for distance class k was tested at the $\alpha' = 0.05/k$ level. Spatial correlation coefficients are not reported for distance classes 15 and 16 (60 and 10 pairs, respectively) because they only include the pairs of points bordering the surface, to the exclusion of all other pairs.

There is a correspondence between individual significant spatial correlation coefficients and the main elements of the spatial structure. The correspondence can clearly be seen in this example, where the data generating process is known. This is not the case when analysing field data, for which the existence and nature of the spatial structures must be confirmed by mapping the data. The presence of several equispaced patches produces an alternation of significant positive and negative values along the correlograms. The first spatial correlation coefficient, which is above 0 in Moran's correlogram and below 1 in Geary's, indicates positive spatial correlation in the first distance class; the first class contains the 420 pairs of points that are at distance 1 of each other on the grid (i.e. the first neighbours in the N-S or E-W directions of the map). Positive and significant spatial correlation in the first distance class confirms that the distance between first neighbours is smaller than the patch size; if the distance between first neighbours in this example were larger than the patch size, the first neighbours would be dissimilar in values and the correlation would be negative for the first distance class. The next peaking positive correlation value (which is smaller than 1 in Geary's correlogram) occurs at distance class 5, which includes distances from 4.95 to 6.19 in grid units; this corresponds to positive spatial correlation between points located at similar positions on neighbouring bumps, or neighbouring troughs; distances between successive peaks are 5 grid units in the E-W or N-S directions. The next peaking positive spatial correlation value occurs at distance class 9 (distances from 9.90 to 11.14 in grid units); it includes value 10, which is the distance between second-neighbour bumps in the N-S and E-W directions. Peaking negative correlation values (which are larger than 1 in Geary's correlogram) are interpreted in a similar way. The first such value occurs at distance class 3 (distances from 2.48 to 3.71 in grid units); it includes value 2.5, which is the distance between peaks and troughs in the N-S and E-W directions on the map. If the bumps were unevenly spaced, the correlograms would be similar for the small distance classes, but there would be no other significant values afterwards.

The main problem with all-directional correlograms is that the diagonal comparisons are included in the same calculations as the N-S and E-W comparisons. As distances become larger, diagonal comparisons between, say, points located near the top of the nine bumps tend to fall in different distance classes than comparable N-S or E-W comparisons. This blurs the signal and makes the spatial correlation coefficients for larger distance classes less significant and interpretable.

2. Wave (Fig. 13.5b). — Each crest was generated as a normal curve. Crests were separated by five grid units; the surface was constructed in this way to make it comparable to Fig. 13.5a. The correlograms are nearly indistinguishable from those of the nine bumps. All-directional

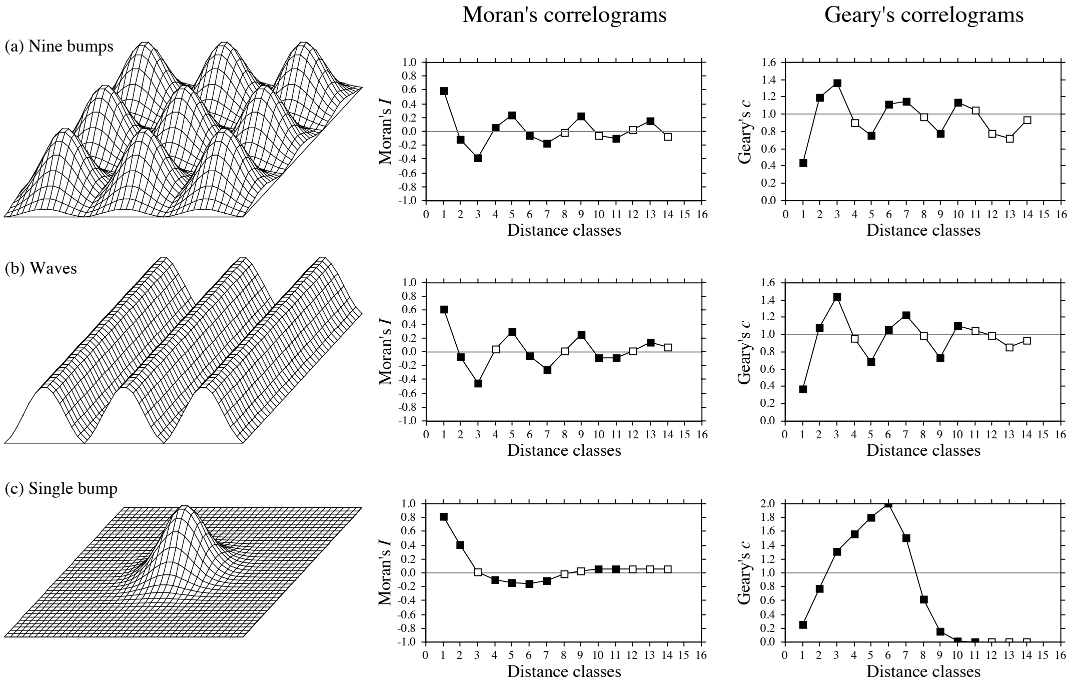

Figure 13.5 Spatial correlation analysis of artificial spatial structures shown on the left: (a) nine bumps; (b) waves; (c) a single bump. Centre and right: all-directional correlograms. Dark squares: correlation statistics that remain significant after progressive Bonferroni correction ($\alpha = 0.05$); white squares: non-significant values. (The figure continues next page.)

correlograms alone cannot tell apart regular bumps from regular waves; directional correlograms or maps are required.

3. Single bump (Fig. 13.5c). — One of the normal curves of Fig. 13.5a was plotted alone at the centre of the study area. Significant negative spatial correlation, which reaches distance classes 6 or 7, delimits the extent of the "range of influence" of this single bump, which covers half the study area. It is not limited here by the rise of adjacent bumps, as this was the case in (a).

4. Linear gradient (Fig. 13.5d). — The correlogram is monotonic decreasing. Nearly all spatial correlation values in the correlograms are significant.

True, false gradient

There are actually two kinds of gradients (Legendre, 1993). *True gradients*, on the one hand, are deterministic structures. Model 1 of Subsection 1.1.1 (induced spatial dependence, eq. 1.1) can generate a true gradient; see Fig. 1.5, case 4. That gradient can be modelled using trend-surface analysis (Subsection 13.2.1). The observed values have independent error terms,

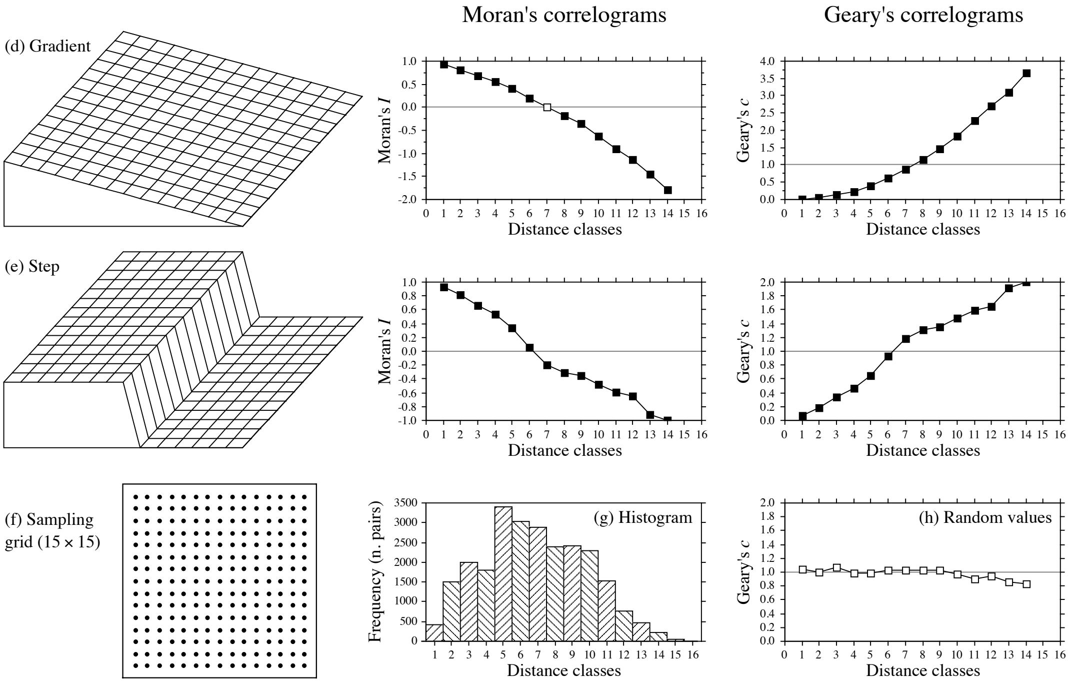

Figure 13.5 **(continued)** Spatial correlation analysis of artificial spatial structures shown on the left: (d) gradient; (e) step. (h) All-directional correlogram of random values. (f) Sampling grid used on each of the artificial spatial structures to obtain 225 "observed values" for spatial correlation analysis. (g) Histogram showing the number of pairs in each distance class. Distances, from 1 to 19.8 in units of the sampling grid, were grouped into 16 distance classes. Spatial correlation statistics (I or c) are not shown for distance classes 15 and 16; see text.

i.e. error terms that are not autocorrelated. *False gradients*, on the other hand, are structures that look like gradients, but actually correspond to spatial correlation generated by some spatial process. Model 2 of Subsection 1.1.1 (spatial autocorrelation, eq. 1.2) can generate a false gradient, especially when the sampling area is small relative to the range of influence of the generating process; see Fig. 1.5, case 3.

In the case of "true gradients", spatial correlation coefficients should not be tested for significance because the condition of second-order stationarity is not satisfied (definition in Subsection 13.1.1); the expected value of the mean is not the same over the whole study area. In the case of "false gradients", however, tests of significance are warranted. For descriptive purposes, correlograms may still be computed for "true gradients" (without tests of significance) because intrinsic stationarity is satisfied. One may also choose to extract a "true gradient" using trend-surface analysis, compute residuals, and look for spatial correlation among the residuals. This is equivalent to trend extraction prior to time series analysis (Section 12.2).

How does one know whether a gradient is "true" or "false"? This is a moot point. When the process generating the observed structure is known, one may decide whether it is likely to have generated spatial correlation in the observed data, or not. Otherwise, one may empirically look at the *target population* of the study. In the case of a spatial study, this is the population of potential sites in the larger area into which the study area is embedded, the study area representing the *statistical population* about which inference can be made. Even from sparse or indirect data, a researcher may form an opinion as to whether the observed gradient is deterministic ("true gradient") or is part of a landscape displaying spatial correlation at broader spatial scale ("false gradient").

5. Step (Fig. 13.5e). — A step between two flat surfaces is enough to produce a correlogram that is indistinguishable, for all practical purposes, from that of a gradient. Correlograms alone cannot tell apart regular gradients from steps; maps are required. As in the case of gradients, there are "true steps" (deterministic) and "false steps" (resulting from an autocorrelated process), although the latter is rare. The presence of a sharp discontinuity in a surface generally indicates that the two parts should be subjected to separate analyses. The methods of boundary detection and constrained clustering (Section 13.3) may help detect such discontinuities and delimit homogeneous areas prior to spatial correlation analysis.

6. Random values (Fig. 13.5h). — Random numbers drawn from a standard normal distribution were generated for each point of the grid and used as the variable to be analysed. Random data are said to represent a "pure nugget effect" in geostatistics. The spatial correlation coefficients were small and non-significant at the 5% level. Only the Geary correlogram is presented.

Sokal (1979) and Cliff & Ord (1981) described, in general terms, where to expect significant values in correlograms, for some spatial structures such as gradients and large or small patches. Their summary tables are in agreement with the test examples above. The absence of significant coefficients in a correlogram must be interpreted with caution, however.

- The absence may indicate that the surface under study is free of spatial correlation at the study scale. This conclusion is subject to *type II error*. Type II error depends on the power of the test, which is a function of (1) the α significance level, (2) the size of effect (i.e. the minimum amount of spatial correlation) one wants to detect, (3) the number of observations (n), and (4) the variance of the sample of data (Cohen, 1988):

$$\text{Power} = (1 - \beta) = f(\alpha, \text{size of effect}, n, s_x^2)$$

Is the test powerful enough to warrant such a conclusion? Are there enough observations to reach significance? The easiest way to increase the power of a test, for a given variable and fixed α, is to increase n.

- The absence may also indicate that the sampling design is inadequate to detect the spatial correlation that may exist in the system. Are the grain size, extent and sampling interval (Section 13.0) adequate to detect the type of spatial correlation one can hypothesize from knowledge about the biological or ecological process under study?

Ecologists can often formulate hypotheses about the mechanism or process that may have generated a spatial phenomenon and deduct the shape that the resulting surface should have. When the model specifies a value for each geographic position (e.g. a spatial gradient), data and model can be compared by correlation analysis. In other instances, the biological or ecological model only specifies the process generating the spatial correlation, not the exact geographic position of each resulting value. Correlograms may be used to support or reject a biological or ecological hypothesis. As in the examples of Fig. 13.5, one can construct an artificial model-surface corresponding to the hypothesis, compute a correlogram of that surface, and compare the correlograms of the real and model data. For instance, Sokal *et al*. (1997a) generated data corresponding to several gene dispersion mechanisms in populations and showed the kind of spatial correlogram that may be expected from each model. Another application concerning phylogenetic patterns of human evolution in Eurasia and Africa (space-time model) is found in Sokal *et al*. (1997b).

Bjørnstad *et al*. (1999) and Bjørnstad & Falck (2001) proposed a spline correlogram, which provides a continuous and model-free function for the spatial covariance. The spline correlogram may be seen as a modification of the nonparametric covariance function of Hall and co-workers (Hall & Patil, 1994; Hall *et al*., 1994). A bootstrap algorithm estimates a confidence envelope around the entire correlogram. Confidence envelopes allow one to test the similarity between correlograms of real or simulated data. See package NCF in Section 13.6.

Ecological application 13.1a

During a study of the factors potentially responsible for the choice of settling sites of *Balanus crenatus* larvae (Cirripedia) in the St. Lawrence Estuary (Hudon *et al*., 1983), plates of artificial substrate (plastic laminate) were subjected to colonization in the infralittoral zone. Plates were positioned vertically, parallel to one another. Pictures of plates were taken during the course of the study. The present ecological application uses data obtained from a picture of a plate taken after a 3-month immersion at a depth of 5 m below low tide, during the summer 1978. The picture was divided into a (10 × 15) grid, for a total of 150 pixels of 1.7 × 1.7 cm. Barnacles were counted by C. Hudon and P. Legendre for the present application (Fig. 13.6a; not published in *op. cit*.). The hypothesis to be tested was that barnacles had a patchy distribution. Barnacles are gregarious animals; their larvae are chemically attracted to settling sites by arthropodine secreted by settled adults (Gabbott & Larman, 1971).

A gradient in larval concentration was expected in the top-to-bottom direction of the plate because of the known negative phototropism of barnacle larvae at the time of settlement (Visscher, 1928). Some kind of border effect was also expected because access to the centre of the plates located in the middle of the pack was more limited than to the fringe. These large-scale effects create violations to the condition of second-order stationarity. A trend-surface equation (Subsection 13.2.1) was computed to account for it, using only the Y coordinate (top-to-bottom axis). Indeed, a significant trend surface was found, involving Y and Y^2, that accounted for 10% of the variation. It forecasted high barnacle concentration in the bottom part of the plate and near the upper and lower margins. Residuals from this equation were calculated and used in spatial correlation analysis.

Euclidean distances were computed among pixels; following Sturge's rule (eq. 13.3), the distances were divided into 14 classes (Fig. 13.6b). Significant positive spatial correlation was

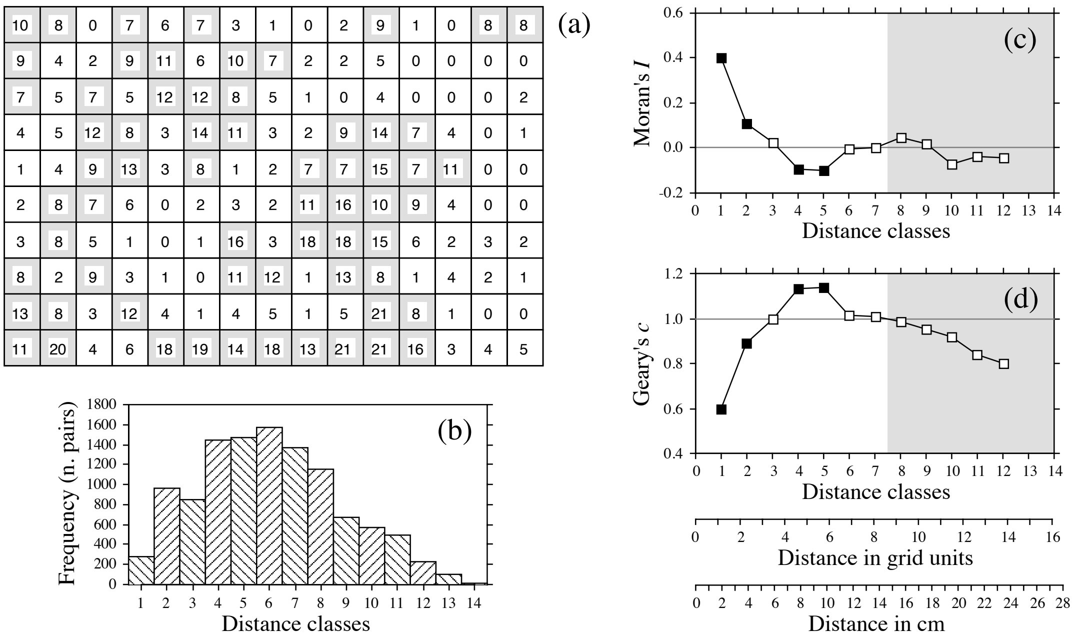

10	8	0	7	6	7	3	1	0	2	9	1	0	8	8
9	4	2	9	11	6	10	7	2	2	5	0	0	0	0
7	5	7	5	12	12	8	5	1	0	4	0	0	0	2
4	5	12	8	3	14	11	3	2	9	14	7	4	0	1
1	4	9	13	3	8	1	2	7	7	15	7	11	0	0
2	8	7	6	0	2	3	2	11	16	10	9	4	0	0
3	8	5	1	0	1	16	3	18	18	15	6	2	3	2
8	2	9	3	1	0	11	12	1	13	8	1	4	2	1
13	8	3	12	4	1	4	5	1	5	21	8	1	0	0
11	20	4	6	18	19	14	18	13	21	21	16	3	4	5

Figure 13.6 (a) Counts of adult barnacles in 150 (1.7 × 1.7 cm) pixels on a plate of artificial substrate (17 × 25.5 cm). The mean concentration is 6.17 animals per pixel; pixels with counts ≥ 7 are shaded to display the aggregates. (b) Histogram of the number of pairs in each distance class. (c) Moran's correlogram. (d) Geary's correlogram. Dark squares: spatial correlation statistics that remain significant after progressive Bonferroni correction ($\alpha = 0.05$); white squares: non-significant values. Grey zones: coefficients that should not be interpreted because they exclude some points in the centre of the study area. Coefficients for distance classes 13 and 14 are not given because they only include the pairs of points bordering the surface. Distances are also given in grid units and in cm.

found in the first distance classes of the correlograms (Fig. 13.6c, d), supporting the hypothesis of patchiness. The size of the patches, or "range of influence" (i.e. the distance between zones of high and low concentrations), is indicated by the distance at which the first maximum negative Moran's *I* correlation value is found. This occurs in classes 4 and 5, which correspond to a distance of about 5 in grid units, or 8 to 10 cm. The patches of high concentration are shaded on the map of the plate of artificial substrate (Fig. 13.6a).

A spatial correlogram is an overall function of spatial correlation across a study area. It is not meant to display details of the structure across the area. Anselin (1995) proposed to decompose the global spatial correlation coefficients into *Local Indicators of Spatial Association* (LISA), producing a local statistic for each sampling unit compared to its surrounding units. LISA can be computed using Moran's *I* or Geary's *c* formulas (eqs. 13.1 and 13.2), and the resulting values can be plotted on maps. Fortin & Dale (2005) give examples of such maps of LISA computed for

LISA

simulated data. Readers can also run the example provided in the documentation file of function ***lisa()*** of package NCF in R.

In anisotropic situations, directional correlograms should be computed in two or several directions. Description of how the pairs of points are chosen is deferred to Subsection 13.1.3 on variograms. One may choose to represent either a single, or several of these correlograms, one for each of the aiming geographic directions, as seems fit for the problem at hand. A procedure for representing in a single figure the directional correlograms computed for several directions of a plane was proposed by Oden & Sokal (1986); Legendre & Fortin (1989) gave an example for vegetation data. Another method is illustrated in Rossi *et al*. (1992).

Another way to approach anisotropic problems is to compute two-dimensional spectral analysis. This method, described by Priestley (1964), Rayner (1971), Ford (1976), Ripley (1981) and Renshaw & Ford (1984), differs from spatial correlation analysis in the structure function it uses. As in time-series spectral analysis (Section 12.5), the method assumes the data to be stationary (second-order stationarity; i.e. no "true gradient" in the data) and made of a combination of sine patterns. A spatial correlation function $r_{dX,dY}$ for all combinations of lags (dX, dY) in the two geographic axes of a plane, as well as a periodogram with intensity I for all combinations of frequencies in the two directions of the plane, are computed. Details of the calculations are also given in Legendre & Fortin (1989), with an example.

3 — Variogram

Like correlograms, semi-variograms (called *variograms* for simplicity) decompose the spatial (or temporal) variability of observed variables among distance classes. The structure function plotted as the ordinate, called *semi-variance*, is the numerator of eq. 13.2:

$$\gamma(d) = \frac{1}{2W(d)} \sum_{h=1}^{n} \sum_{i=1}^{n} w_{hi} (y_h - y_i)^2 \quad \text{for } h \neq i \tag{13.9}$$

or, for symmetric distance and weight matrices, which is the most common case:

$$\gamma(d) = \frac{1}{2W(d)} \sum_{h=1}^{n-1} \sum_{i=h+1}^{n} w_{hi} (y_h - y_i)^2 \tag{13.10}$$

$\gamma(d)$ is thus a non-standardized form of Geary's c coefficient. γ may be seen as a measure of the error mean square of the estimate of y_i using a value y_h distant from it by d. The two equation forms produce the same numerical value in the case of symmetric distance and weight matrices. The calculation is repeated for different values of d. This provides the *sample variogram*, which is a plot of the empirical values of variance $\gamma(d)$ as a function of distance d.

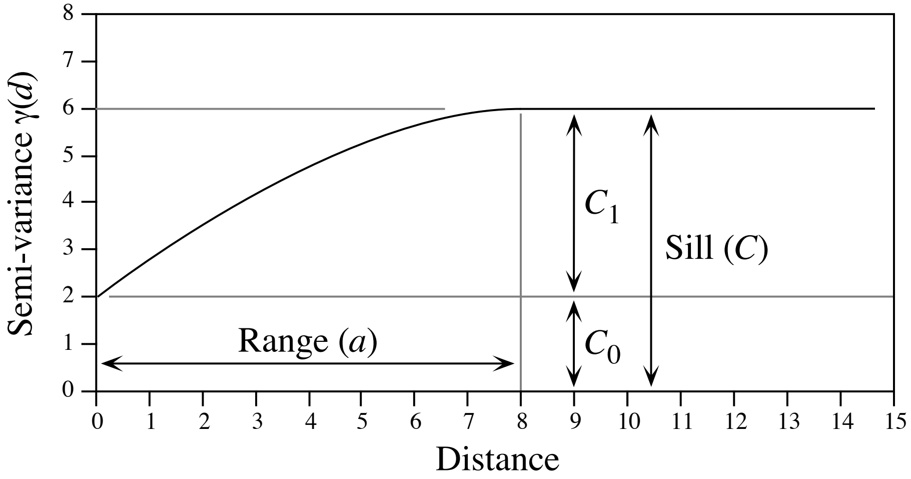

Figure 13.7 Spherical variogram model showing characteristic features: nugget effect ($C_0 = 2$ in this example), spatially structured component ($C_1 = 4$), sill ($C = C_0 + C_1 = 6$), and range ($a = 8$).

The equations usually found in the geostatistical literature look a bit different, but they correspond to the same calculations and give the same results:

$$\gamma(d) = \frac{1}{2W(d)} \sum_{i=1}^{W(d)} (y_i - y_{i+d})^2 \qquad \text{or} \qquad \gamma(d) = \frac{1}{2W(d)} \sum_{(h,i)\,|\,d_{hi} \approx d}^{W(d)} (y_h - y_i)^2$$

Both of these expressions mean that pairs of values are selected to be at distance d of each other; there are $W(d)$ such pairs for any given distance class d. The condition $d_{hi} \approx d$ means that distances may be grouped into distance classes, placing in class d the individual distances d_{hi} that are approximately equal to d. In directional variograms (below), d is a directional measure of distance, i.e. taken in a specified direction only. The semi-variance function is often called the variogram in the geostatistical literature. When computing a variogram, one assumes that the spatial correlation function applies to the entire surface under study (intrinsic stationarity, Subsection 13.1.1).

Generally, variograms tend to level off at a *sill* which is equal to the variance of the variable (Fig. 13.7); the presence of a sill implies that the data are second-order stationary. The distance at which the variance levels off is referred to as the *range* (parameter a); beyond that distance, the sampling units are not spatially correlated. The discontinuity at the origin (non–zero intercept) is called the *nugget effect*; the geostatistical origin of the method transpires in that name. It corresponds to the local variation occurring at scales finer than the sampling interval, such as sampling error, fine-scale spatial variability, and measurement error. The nugget effect is represented

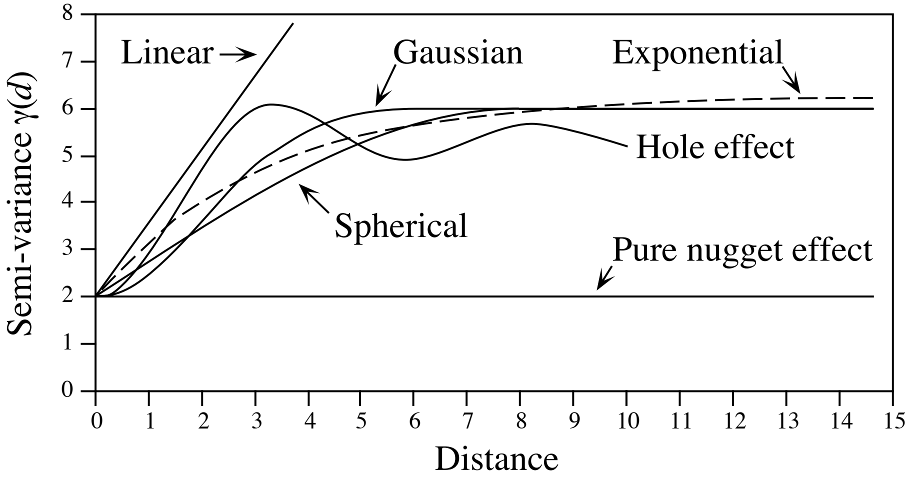

Figure 13.8 Commonly used variogram models.

by the error term ε_{ij} in spatial structure model 2 (eq. 1.2) of Subsection 1.1.1. It describes a portion of variation which is not autocorrelated, or is autocorrelated at a scale finer than can be detected by the sampling design. The parameter for the nugget effect is C_0 and the spatially structured component is represented by C_1; the sill, C, is equal to $C_0 + C_1$. The *relative nugget effect* is $C_0/(C_0 + C_1)$.

Although a sample variogram is a good descriptive summary of the spatial contiguity of a variable, it does not provide all the semi-variance values needed for kriging (Subsection 13.2.2). A model must be fitted to the sample variogram; the model will provide values of semi-variance for all the intermediate distances. The most commonly used models are the following (Fig. 13.8):

- Spherical model: $\gamma(d) = C_0 + C_1\left[1.5\frac{d}{a} - 0.5\left(\frac{d}{a}\right)^3\right]$ if $d \le a$; $\gamma(d) = C$ if $d > a$;

- Exponential model: $\gamma(d) = C_0 + C_1\left[1 - \exp\left(-3\,\frac{d}{a}\right)\right]$;

- Gaussian model: $\gamma(d) = C_0 + C_1\left[1 - \exp\left(-3\,\frac{d^2}{a^2}\right)\right]$;

- Hole effect model: $\gamma(d) = C_0 + C_1\left[1 - \frac{\sin(ad)}{ad}\right]$. An equivalent form is $\gamma(d) = C_0 + C_1\left[1 - \frac{a'\sin(d/a')}{d}\right]$ where $a' = 1/a$. $(C_0 + C_1)$ represents the value of γ towards which the dampening sine function tends to stabilize. This equation would adequately model a variogram of the periodic structures in Fig. 13.5a-b (variograms only differ from Geary's correlograms by the scale of the ordinate);

- Linear model: $\gamma(d) = C_0 + bd$ where b is the slope of the variogram model. A linear model with sill is obtained by adding the specification: $\gamma(d) = C$ if $d \geq a$;

- Pure nugget effect model: $\gamma(d) = C_0$ if $d > 0$; $\gamma(d) = 0$ if $d = 0$. The latter part applies to a point estimate. In practice, observations have the size of the sampling grain (Section 13.0); the error at that scale is always larger than 0.

Other less-frequently encountered variogram models are described in geostatistics textbooks. A model is usually chosen on the basis of the known or assumed process having generated the spatial structure. Several models may be added up to fit any particular sample variogram. Parameters may be fitted by weighted least squares; the weights are functions of the distance and the number of pairs in each distance class (Cressie, 1991); in practice, variograms are often fitted by visual estimation. Fitting a variogram model requires that the hypothesis of intrinsic stationarity be satisfied (Subsection 13.1.1).

Anisotropy

As mentioned at the beginning of Subsection 13.1.2, anisotropy is present in data when the spatial correlation function is not the same for all geographic directions considered (David, 1977; Isaaks & Srivastava, 1989). In *geometric anisotropy*, the variation to be expected between two sites distant by d in one direction is equivalent to the variation expected between two sites distant by $b \times d$ in another direction. The range of the variogram changes with direction while the sill remains constant. In a river for instance, the kind of variation expected in phytoplankton concentration between two sites 5 m apart across the current may be the same as the variation expected between two sites 50 m apart along the current even though the variation can be modelled by spherical variograms with the same sill in the two directions. Constant b is called the *anisotropy ratio* (b = 50/5 = 10 in the river example). This is equivalent to a change in distance units along one of the axes. The anisotropy ratio may be represented by an ellipse or a more complex figure on a map, its axes being proportional to the variation expected in each direction. In *zonal anisotropy*, the sill of the variogram changes with direction while the range remains constant. An extreme case is offered by a strip of land. If the long axis of the strip is oriented in the direction of a major environmental gradient, the variogram may correspond to a linear model (always increasing) or to a spherical model with a sill larger than the nugget effect, whereas the variogram in the direction perpendicular to it may show only random variation without spatial structure with a sill equal to the nugget effect.

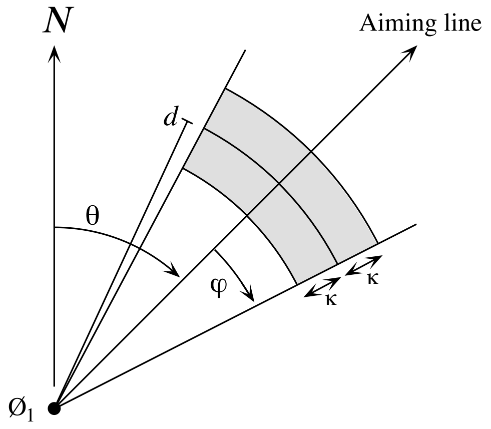

Figure 13.9 Search parameters for pairs of points in directional variograms and correlograms. From an observed study site $Ø_1$, an aiming line is drawn in the direction determined by angle θ (usually by reference to the geographic north, indicated by *N* in the figure). The angular tolerance parameter φ determines the search zone (grey) laterally whereas parameter κ sets the tolerance along the aiming line for each distance class *d*. Points within the search window (in gray) are included in the calculation of $I(d)$, $c(d)$ or $\gamma(d)$.

Directional variogram and correlogram

Directional variograms and correlograms may be used to determine whether anisotropy (defined in Subsection 13.1.2) is present in data; they may also be used to describe anisotropic surfaces or to account for anisotropy in kriging (Subsection 13.2.2). A direction of space is chosen (i.e. an angle θ, usually by reference to the geographic north) and a search is launched for the pairs of points that are within a given distance class *d* in that direction. There may be few such pairs perfectly aligned in the aiming direction, or none at all, especially when the observed sites are not regularly spaced on the map. More pairs can usually be found by looking within a small neighbourhood around the aiming line (Fig. 13.9). The neighbourhood is determined by an angular tolerance parameter φ and a parameter κ that sets the tolerance for distance classes along the aiming line. For each observed point $Ø_h$ in turn, one looks for other points $Ø_i$ that are at distance $d \pm \kappa$ from it. All points found within the search window are paired with the reference point $Ø_h$ and included in the calculation of semi-variance or spatial correlation coefficients for distance class *d*. In most applications, the search is bi-directional, meaning that one also looks for points within a search window located in the direction opposite (180°) the aiming direction. Isaaks & Srivastava (1989, their Chapter 7) propose a way to assemble directional measures of semi-variance into a single table and produce a contour map that describes the anisotropy in the data, if any; Rossi *et al.* (1992) have used the same approach for directional spatial correlograms.

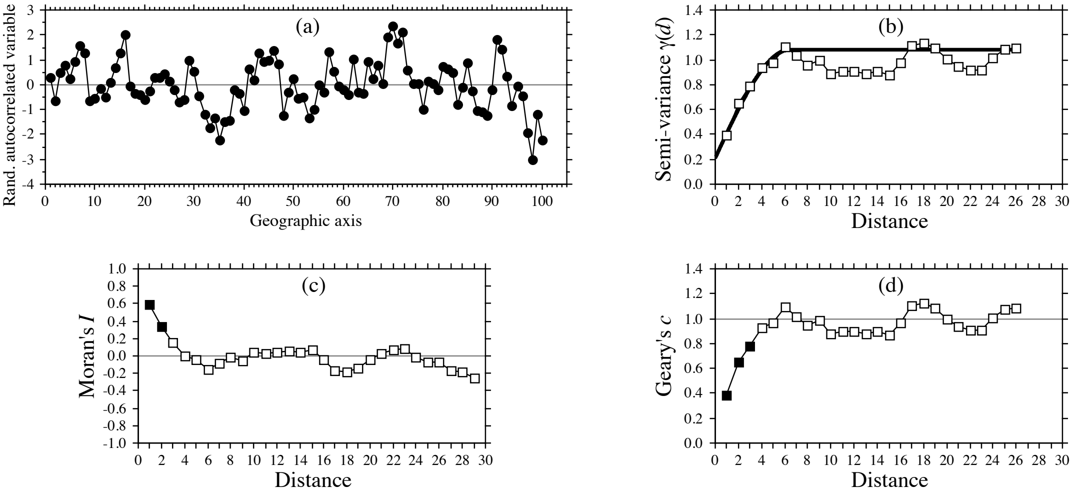

Figure 13.10 (a) Series of 100 equispaced random, spatially autocorrelated data. (b) Sample variogram, with spherical model superimposed (heavy line). Abscissa: distances between points along the geographic axis in (a). (c-d) Spatial correlograms. Dark squares: spatial correlation statistics that remain significant after progressive Bonferroni correction ($\alpha = 0.05$); white squares: non-significant values.

Numerical example. An artificial data set was produced containing random autocorrelated data (Fig. 13.10a). The data were generated using the turning bands method (David, 1977; Journel & Huijbregts, 1978); random normal deviates were autocorrelated following a spherical model with a range of 5. The sample variogram (without test of significance) and spatial correlograms (with tests) are shown in Fig. 13.10b-d. In this example, the data were standardized during data generation, so that the denominator of eq. 13.2 was 1; therefore, the sample variogram and Geary's correlogram were identical. The variogram suggests a spherical model with a range of 6 units and a small nugget effect (Fig. 13.10b).

Besides the description of spatial structures, variograms are used for several other purposes in spatial analysis. In Subsection 13.2.2, they will be the basis for interpolation by kriging. In addition, structure functions (variograms, spatial correlograms) may prove extremely useful to help determine the grain size of the sampling units and the sampling interval to be used in a survey, based upon the analysis of a pilot study. They may also be used to perform change-of-scale operations and predict the type of spatial correlation and variance that would be observed if the grain size of the sampling design were different from that actually used in a field study (Bellehumeur *et al.*, 1997).

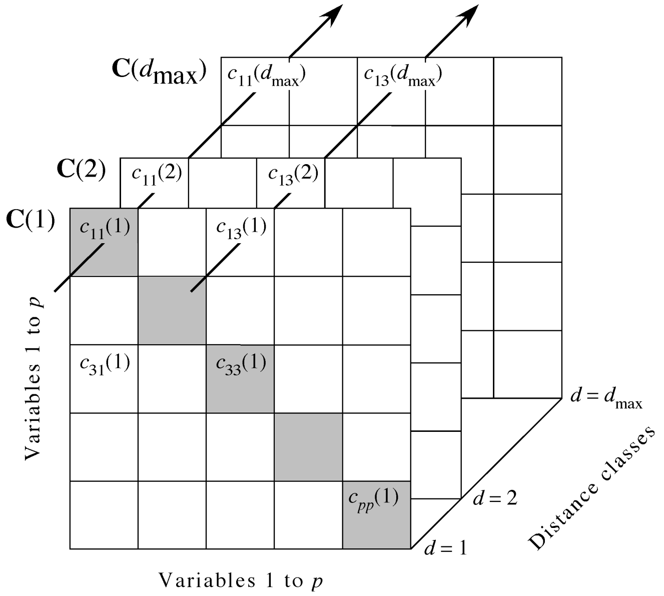

Figure 13.11 Representation of a variogram matrix **C** containing the information from all variograms and cross-variograms. **C** is composed of separate variance-covariance matrices **C**(d), each of size (p × p), corresponding to one of the distance classes d. Redrawn from Wagner (2003).

4 — Multivariate variogram

Consider a multivariate matrix **Y** with n rows (sites) and p columns, e.g. species presence-absence or abundance data. A variogram $\gamma_j(d)$ for a single variable j is computed using eq. 13.10. The cross-variogram $\gamma_{jk}(d)$ between two variables j and k is now defined as follows (Isaaks & Srivastava, 1989):

$$\gamma_{jk}(d) = \frac{1}{2W(d)} \sum_{(h,i)\,|\,d_{hi} \approx d}^{W(d)} (y_{jh} - y_{ji})\,(y_{kh} - y_{ki}) \qquad \textbf{(13.11)}$$

It partitions the covariance between two variables among the distance classes d.

Each variogram and cross-variogram can be seen as a vector containing values computed for different distance classes; the largest distance class is labelled d_{max}. For a multivariate response matrix **Y** of size (n × p), a variogram is produced for each of the p variables and there is a cross-variogram for each of the $p(p-1)/2$ pairs of variables. These vectors can be assembled in a distance-dependent cubic symmetric variance-covariance matrix called the *variogram matrix* **C** (Myers, 1997; Fig. 13.11) with elements $c_{ij}(d) = \gamma_{jk}(d)$ (eq. 13.11). The arrows in the figure show the values

Variogram matrix

$c_{11}(d)$ used to draw the variogram $\gamma_{11}(d)$ of variable 1 and the values $c_{13}(d)$ used to draw the cross-variogram $\gamma_{13}(d)$ crossing variables 1 and 3.

Matrix **C** contains a series of square variance-covariance matrices $\mathbf{C}(d)$. Each matrix $\mathbf{C}(d)$ is of size $(p \times p)$ because it is computed among the p descriptors; it contains the information for one of the distance classes d of each variogram and cross-variogram. The variance-covariance matrix $\mathbf{S_Y}$ of the p-dimensional matrix **Y** is the weighted sum of the $\mathbf{C}(d)$ matrices, showing that the set of $\mathbf{C}(d)$ matrices represents an additive decomposition of the total variance-covariance matrix $\mathbf{S_Y}$ among the distance classes d. The weights in that sum are the number of pairs of points used to compute the values in each distance class divided by the total number of pairs of points.

In order for the variances of the variables in data matrix **Y** to be additive, these must be in the same physical dimensions or standardized. This question was discussed in the first paragraph of Subsection 9.1.5. The variogram matrix can be used to plot several graphs (Wagner, 2003):

- The empirical variogram of variable j is obtained by plotting the diagonal elements $c_{jj}(d)$ (e.g. the values along the left-hand arrow in Fig. 13.11) against distances d.

- The empirical cross-variogram of variables j and k is obtained by plotting the non-diagonal elements $c_{jk}(d)$ (e.g. the values along the right-hand arrow in Fig. 13.11) against distances d.

- Sum the diagonal elements (gray squares in Fig. 13.11) in each matrix $\mathbf{C}(d)$. Since the sum of the diagonal elements of **S** is the total variance in **Y** and the matrices $\mathbf{C}(d)$ decompose **S**, a plot of these sums against distances d is the *multivariate variogram* decomposing the total variance in **S**. An example is given in Ecological application 13.1b. Furthermore, Wagner (2003) showed that for species presence-absence data, a plot of these sums against distances d is an empirical *variogram of complementarity*, meaning the variogram of the dissimilarity in species composition. These sums are direct measures of species turnover between sites located at distances d; a higher sum of variances indicates larger differences among the sites separated by that distance than for other distances where the among-site sum of variances is lower.

Multivariate variogram

- As shown in Section 4.1, the sum of all values in matrix **S** is equal to the variance of a new variable, **y**, computed as the sum by rows of all variables in **Y**. Because the matrices $\mathbf{C}(d)$ represent a decomposition of **S** among the distance classes d, one can sum all elements of each matrix $\mathbf{C}(d)$ and plot these sums against distances d to obtain a variogram of **y**. If **Y** contains species abundance data, the graph is a variogram of the total number of individuals at the sites, which can in some cases be interpreted as the total yield or the carrying capacity of the sites. If **Y** comprises species presence-absence data, a variogram of species richness is obtained (Wagner, 2003).

The statistics in multivariate variograms can be tested for significance using Mantel tests (Wagner, 2004). The tests used in function ***mso()*** of VEGAN in R, which

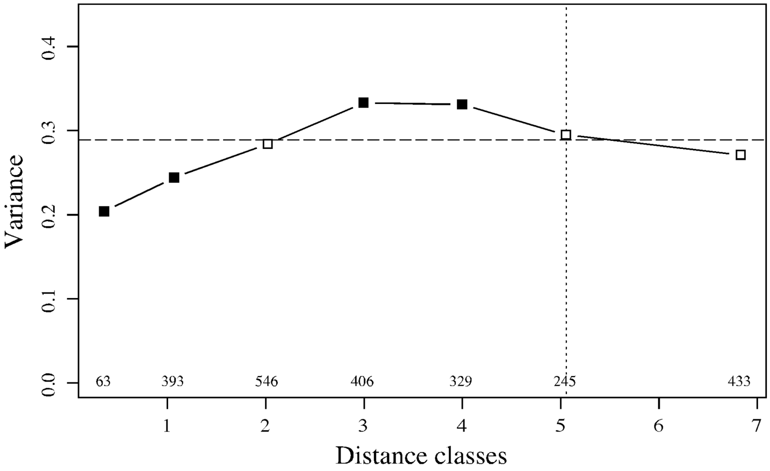

Figure 13.12 Multivariate variogram of the Hellinger-transformed and detrended mite data, computed using function ***mso()***. Dark squares: variances with p-values significant at the 5% level, after Bonferroni correction for 7 simultaneous tests. Dashed horizontal line: total variance in the data. Vertical dotted line: half the maximum number of classes; the last point, to the right of that line, includes all remaining pairs of sites and should not be interpreted. Values written above the abscissa: number of pairs involved in the calculation of each statistic.

are based on the matrix of squared distances, are identical to those used in the Mantel correlogram (Subsection 13.1.6).

Ecological application 13.1b

The oribatid mite data of Borcard & Legendre (1994), analysed in Ecological application 11.5, are used here to compute a multivariate variogram. Prior to analysis, the mite data were Hellinger-transformed (eq. 7.69) and detrended along the north-south axis of the study area to meet the stationarity assumption. Function ***mso()*** of the R VEGAN package was used to compute the variogram; see Section 13.6.

The results are shown in Fig. 13.12. The interval size of the distance classes was the distance that kept all points connected in a dbMEM analysis; this is the threshold distance (*thresh*) of Section 14.1, 1.01119 m. The horizontal line in Fig. 13.12 is the total variance in the data. It is also the weighted sum of the variances (sums of the diagonal elements) of the $\mathbf{C}(d)$ matrices over the different distance classes. Because the sum of the weights is 1, as explained in the description of the method, the dashed line is located at the weighted mean of the multivariate variogram values and can be used as a reference for their visual assessment.

The p-values were Bonferroni-corrected for 7 simultaneous tests. The variogram displays significant spatial correlation; it may correspond to a spherical or a hole model. These data will be further analysed by multiscale ordination in Section 14.4.

5 — Spatial covariance, semi-variance, correlation, cross-correlation

This subsection examines the relationships between spatial covariance, semi-variance and correlation (including cross-correlation), under the assumption of second-order stationarity, leading to the concept of cross-correlation. The assumption of second-order stationarity (Subsection 13.1.1) may be restated as follows:

- The first moment (mean of values *i*) of the variable has a constant and finite value:

$$\mathrm{E}[y_i] = \frac{1}{n}\sum_{i=1}^{n} y_i = m_i \qquad \textbf{(13.12)}$$

and its value does not depend on the position in the study area.

- The second moment (spatial covariance, numerator of eq. 13.1) of the variable exists (i.e. the variogram has a finite sill value):

$$C(d) = \left[\frac{1}{W(d)} \sum_{(h,\,i)\,|\,d_{hi} \approx d}^{W(d)} y_h y_i\right] - m_h m_i \qquad \textbf{(13.13)}$$

$$C(d) = \mathrm{E}[y_h y_i] - m^2 \quad \text{for } h, i \,|\, d_{hi} \approx d \qquad \textbf{(13.14)}$$

$h, i \,|\, d_{hi} \approx d$ means that the pairs of points h and i used to compute covariance $C(d)$ are at distances d_{hi} that are approximately equal to d. The values of $C(d)$ depend only on d and on the orientation of the distance vectors, not on their positions in the study area.

To understand eq. 13.13 as a measure of covariance, imagine the elements of the various pairs y_h and y_i written in two columns as if they were two variables. The equation for the covariance (eq. 4.4) may be written as follows, using a final division by n instead of $(n-1)$ (maximum-likelihood estimate of the covariance, which is standard in geostatistics):

$$s_{y_h y_i} = \frac{\sum y_h y_i}{n} - \frac{\sum y_h}{n}\frac{\sum y_i}{n} = \frac{\sum y_h y_i}{n} - m_h m_i$$

The overall variance (Var[y_i], with division by n instead of $n-1$) also exists since it is the covariance calculated for $d = 0$:

$$\mathrm{Var}[y_i] = \mathrm{E}[y_i - m_i]^2 = C(0) \qquad \textbf{(13.15)}$$

When computing the semi-variance, one only considers pairs of observations distant by d. Equations 13.9 and 13.10 are re-written as follows:

$$\gamma(d) = 0.5\,\mathrm{E}[y_h - y_i]^2 \quad \text{for } h, i \,|\, d_{hi} \approx d \qquad \textbf{(13.16)}$$

A few lines of algebra obtain the following formula:

$$\gamma(d) = \frac{\sum y_i^2 - \sum y_h y_i}{W(d)} = C(0) - C(d) \quad \text{for } h, i \mid d_{hi} \approx d \qquad \textbf{(13.17)}$$

Two properties are used in the derivation of eq. 13.17 from eq. 3.16: (1) $\sum y_h = \sum y_i$, and (2) the variance (Var[y_i], eq. 13.15) can be estimated using any subset of the observed values if the hypothesis of second-order stationarity is verified.

The correlation is the covariance divided by the product of the standard deviations. For a spatial process, the (auto)correlation is written as follows:

$$r(d) = \frac{C(d)}{s_h s_i} = \frac{C(d)}{\text{Var}[y_i]} = \frac{C(d)}{C(0)} \qquad \textbf{(13.18)}$$

The right-hand formula is Moran's *I* (eq. 13.1). Consider the formula for Geary's *c* (eq. 13.2), which is the semi-variance divided by the overall variance (ignoring the fact that the variance in eq. 13.2 is computed with division by $n - 1$ instead of n). The following derivation

$$c(d) = \frac{\gamma(d)}{\text{Var}[y_i]} = \frac{C(0) - C(d)}{C(0)} = 1 - \frac{C(d)}{C(0)} = 1 - r(d)$$

shows that Geary's *c* is one minus the coefficient of spatial (auto)correlation (ignoring again the division by $n - 1$ instead of n). In a graph, the semi-variance and Geary's *c* coefficient have exactly the same shape (e.g. Fig. 13.10, b and d); only the ordinate scales may differ if Var[y_i] is not 1. An autocorrelogram plotted using $r(d)$ has the exact reverse shape as a Geary correlogram. The important conclusion is that the plots of semi-variance, covariance, Geary's *c* coefficient, and $r(d)$, are equivalent to characterize spatial structures under the hypothesis of second-order stationarity (Bellehumeur & Legendre, 1998).

Cross-covariances may also be computed from eq. 13.13, using values of *two different variables* observed at locations distant by *d* (Isaaks & Srivastava, 1989). Equation 13.18 leads to a formula for cross-correlation that may be used to plot cross-correlograms; the construction of the cross-correlation statistic is the same as for time series (eq. 12.9). With transect data, the result is similar to that of eq. 12.9. However, the programs designed to compute spatial cross-correlograms do not require the data to be equispaced, contrary to programs for time-series analysis. The theory is presented by Rossi *et al.* (1992), as well as applications to ecology.

Ecological application 13.1c

A survey was conducted on a homogeneous sandflat in the Manukau Harbour, New Zealand, to identify the scales at which spatial heterogeneity could be detected in the distribution of adult and juvenile bivalves (*Macomona liliana* and *Austrovenus stutchburyi*), as well as indications of

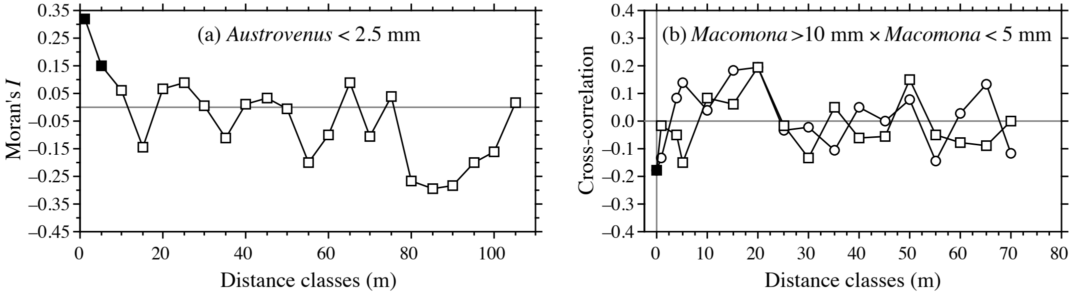

Figure 13.13 (a) Spatial autocorrelogram for juvenile *Austrovenus* densities. (b) Cross-correlogram for adult-juvenile *Macomona* interactions, folded about the ordinate: circles = positive lags, squares = negative lags. Dark symbols: correlation statistics that are significant after progressive Bonferroni correction (α = 0.05). Redrawn from Hewitt *et al.* (1997).

adult-juvenile interactions within and between species. The results were reported by Hewitt *et al.* (1997); see also Ecological application 13.2. Sampling was conducted along transects established at three sites located within a 1-km^2 area; there were two transects at each site, forming a cross. This way, there were transects perpendicular to the direction of tidal flow, and others parallel. Sediment cores (10 cm diam., 13 cm deep) were collected using a nested sampling design; the basic design was a series of cores 5 m apart, but additional cores were taken 1 m from each of the 5-m-distant cores. This design provided several comparisons in the short distance classes (1, 4, 5, and 6 m). Using transects instead of rectangular areas allowed relatively large distances (150 m) to be studied, given the allowable sampling effort. Nested sampling designs have also been advocated by Fortin *et al.* (1989) and by Bellehumeur & Legendre (1998).

Spatial correlograms were used to identify scales of variation in bivalve concentrations. The Moran correlogram for juvenile *Austrovenus*, computed for the three transects perpendicular to the direction of tidal flow, displayed significant spatial correlation at distances of 1 and 5 m (Fig. 13.13a). The same pattern was found in the transects parallel to tidal flow. Figure 13.13a also indicates that the range of influence of spatial correlation was about 15 m. This was confirmed by plotting bivalve concentrations along the transects: LOWESS smoothing of the graphs (Subsection 10.3.8) showed patches of about 25-30 m in diameter (Hewitt *et al.*, 1997, their Figs. 3 and 4).

Cross-correlograms were computed to detect signs of adult-juvenile interactions. In the comparison of adult (> 10 mm) to juvenile *Macomona* (< 5 mm), a significant negative cross-correlation was identified at 0 m in the direction parallel to tidal flow (Fig. 13.13b); correlation was not significant for the other distance classes. As in time series analysis, the cross-correlation function is not symmetrical; the correlation obtained by comparing values of $\mathbf{y}_1$ to values of $\mathbf{y}_2$ located at distance d on their right is not the same as when values of $\mathbf{y}_2$ are compared to values of $\mathbf{y}_1$ located at distance d on their right, except for $d = 0$. In Fig. 13.13b, the cross-correlogram is folded about the ordinate (compare to Fig. 12.9). Contrary to time series analysis, it is not useful in spatial analysis to discuss the direction of lag of a variable with respect to the other unless one has a specific hypothesis to test.

6 — Multivariate Mantel correlogram

Sokal (1986) and Oden & Sokal (1986) found an ingenious way to compute a correlogram for multivariate data, using the normalized Mantel statistic r_M and test of significance (Subsection 10.5.1). This method is useful, in particular, to describe the spatial structure of species assemblages.

The principle is to quantify the ecological relationships among sampling sites by means of a matrix **Y** of multivariate similarities or distances (using, for instance, coefficients S_{17} or D_{14} in the case of species abundance data), and compare **Y** to a *model matrix* **X** (Subsection 10.5.1), which is different for each geographic distance class (Fig. 13.14).

- For distance class 1 for instance, pairs of neighbouring stations (that belong to the first class of geographic distances) are coded 1, whereas the remainder of matrix **X**(1) contains zeros. A first Mantel statistic (r_{M1}) is calculated between **Y** and **X**(1).

- The process is repeated for the other distance classes d, building each time a model-matrix **X**(d) and recomputing the normalized Mantel statistic. Matrix **X**(d) may contain 1's for pairs that are in the given distance class, or the code value for that distance class (d) (as in Fig. 13.14), or any other value different from zero; all coding methods lead to the same value of the normalized Mantel statistic r_M.

The Mantel statistics, plotted against distance classes, produce a multivariate correlogram. Each value is tested for significance in the usual way, using either permutations or Mantel's normal approximation (Box 10.2). Computation of standardized Mantel statistics assumes second-order stationarity. Borcard & Legendre (2012) have shown that for univariate data, the tests of significance in a Mantel correlogram computed on the matrix of *squared* Euclidean distances was equivalent to the tests in a Geary's c correlogram. Using numerical simulations, they also showed that the power of the test in Mantel correlograms was high for multivariate data.

A multivariate correlogram can be computed with function ***mantel.correlog()*** in R; see Section 13.6. If the calculation is based upon a *squared* Euclidean distance matrix, the Mantel test results in the multivariate correlogram are identical to the Mantel test results computed by the multivariate variogram function ***mso()***, provided that the distance classes are the same (Borcard & Legendre, 2012). As in the case of univariate correlograms (above), one is advised to use some form of correction for multiple testing (Box 1.3) before interpreting multivariate correlograms and variograms.

Numerical example. Consider again the 10 sampling sites of Fig. 13.4. Assume that species assemblage data were available and produced similarity matrix **S** of Fig. 13.14. Matrix **S** played here the role of $\mathbf{D_Y}$ in the computation of Mantel statistics. Were the species data autocorrelated? Distance matrix **D**, already divided into 6 classes in Fig. 13.4, was recoded into a series of model matrices **X**(d) (d = 1, 2, etc.). In each of these, the pairs of sites that were in the given distance class received the value d, whereas all other pairs received the value 0. Mantel statistics were computed between **S** and each of the **X**(d) matrices in turn; positive and significant Mantel

$$\mathbf{S} = \begin{bmatrix} 1.00 & 0.56 & 0.35 & 0.55 & 0.71 & 0.76 & 0.39 & 0.40 & 0.29 & 0.75 \\ 0.56 & 1.00 & 0.71 & 0.48 & 0.75 & 0.37 & 0.55 & 0.79 & 0.38 & 0.54 \\ 0.35 & 0.71 & 1.00 & 0.47 & 0.63 & 0.15 & 0.38 & 0.65 & 0.34 & 0.44 \\ 0.55 & 0.48 & 0.47 & 1.00 & 0.69 & 0.43 & 0.31 & 0.34 & 0.46 & 0.73 \\ 0.71 & 0.75 & 0.63 & 0.69 & 1.00 & 0.50 & 0.43 & 0.56 & 0.39 & 0.78 \\ 0.76 & 0.37 & 0.15 & 0.43 & 0.50 & 1.00 & 0.36 & 0.25 & 0.27 & 0.56 \\ 0.39 & 0.55 & 0.38 & 0.31 & 0.43 & 0.36 & 1.00 & 0.65 & 0.60 & 0.27 \\ 0.40 & 0.79 & 0.65 & 0.34 & 0.56 & 0.25 & 0.65 & 1.00 & 0.41 & 0.35 \\ 0.29 & 0.38 & 0.34 & 0.46 & 0.39 & 0.27 & 0.60 & 0.41 & 1.00 & 0.29 \\ 0.75 & 0.54 & 0.44 & 0.73 & 0.78 & 0.56 & 0.27 & 0.35 & 0.29 & 1.00 \end{bmatrix}$$

$$\nearrow \mathbf{X}(1) = \begin{bmatrix} — & & & & & & & & & \\ 0 & — & & & & & & & & \\ 0 & 0 & — & & & & & & & \\ 1 & 0 & 0 & — & & & & & & \\ 0 & 0 & 0 & 1 & — & & & & & \\ 0 & 0 & 0 & 0 & 0 & — & & & & \\ 0 & 0 & 0 & 0 & 0 & 0 & — & & & \\ 0 & 1 & 0 & 0 & 0 & 0 & 0 & — & & \\ 0 & 0 & 0 & 0 & 0 & 0 & 1 & 0 & — & \\ 1 & 0 & 0 & 1 & 1 & 0 & 0 & 0 & 0 & — \end{bmatrix} \quad r_{\mathrm{M}1} = 0.53847$$

$$\mathbf{D} = \begin{bmatrix} — & & & & & & & & & \\ 3 & — & & & & & & & & \\ 5 & 2 & — & & & & & & & \\ 1 & 2 & 4 & — & & & & & & \\ 2 & 2 & 3 & 1 & — & & & & & \\ 2 & 5 & 6 & 3 & 4 & — & & & & \\ 5 & 3 & 5 & 5 & 4 & 5 & — & & & \\ 5 & 1 & 2 & 4 & 3 & 6 & 2 & — & & \\ 4 & 3 & 4 & 4 & 4 & 4 & 1 & 2 & — & \\ 1 & 3 & 4 & 1 & 1 & 3 & 6 & 5 & 5 & — \end{bmatrix} \rightarrow \mathbf{X}(2) = \begin{bmatrix} — & & & & & & & & & \\ 0 & — & & & & & & & & \\ 0 & 2 & — & & & & & & & \\ 0 & 2 & 0 & — & & & & & & \\ 2 & 2 & 0 & 0 & — & & & & & \\ 2 & 0 & 0 & 0 & 0 & — & & & & \\ 0 & 0 & 0 & 0 & 0 & 0 & — & & & \\ 0 & 0 & 2 & 0 & 0 & 0 & 2 & — & & \\ 0 & 0 & 0 & 0 & 0 & 0 & 0 & 2 & — & \\ 0 & 0 & 0 & 0 & 0 & 0 & 0 & 0 & 0 & — \end{bmatrix} \quad r_{\mathrm{M}2} = 0.42007$$

etc.

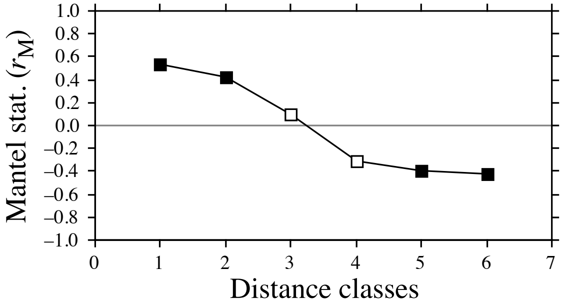

Figure 13.14 Construction of a Mantel correlogram for a similarity matrix **S** ($n = 10$ sites). The matrix of geographic distance classes **D**, from Fig. 13.4d, gives rise to model matrices **X**(1), **X**(2), etc. for the various distance classes d. These are compared, in turn, to matrix **S** using standardized Mantel statistics ($r_{\mathrm{M}d}$). Dark squares in the correlogram: Mantel statistics that are significant after progressive Bonferroni correction ($\alpha = 0.05$).

statistics indicate positive spatial correlation in the present case. The statistics were tested for significance using 999 permutations and plotted against distance classes d to form the Mantel correlogram. The progressive Bonferroni method was used to account for multiple testing because interest was primarily in detecting spatial correlation in the first distance classes.

Before computing the Mantel correlogram, one must assume that the condition of second-order stationarity is satisfied. This condition is more difficult to explain in the case of multivariate data; it means essentially that the surface is uniform in (multivariate) mean, variance and covariance at broad scale. The correlogram illustrated in Fig. 13.14 suggests the presence of a gradient. If the condition of second-order-stationarity is satisfied, this means that the gradient detected by this analysis is a part of a larger, autocorrelated spatial structure. This was called a “false gradient” in the numerical example of Subsection 13.1.2.

When $\mathbf{D_Y}$ is a similarity matrix and distance classes are coded as described above, positive Mantel statistics correspond to positive spatial correlation; this is the case in the numerical example. When the values in $\mathbf{D_Y}$ are distances instead of similarities, or if the 1’s and 0’s are interchanged in matrix **X**, the signs of all Mantel statistics are changed. One should always specify whether positive spatial correlation is expressed by positive or negative values of the Mantel statistics when presenting Mantel correlograms. Mantel correlograms have been computed for real data by Legendre & Fortin (1989), Le Boulengé *et al.* (1996), and Fortin & Dale (2005).

13.2 Maps

The most basic step in spatial pattern analysis is the production of maps displaying the spatial distributions of values of the variable(s) of interest. Furthermore, maps are essential to help interpret spatial structure functions (Section 13.1).

Several methods are available in mapping programs. The final product of modern computer programs may be a contour map, a mesh map (such as Figs. 13.15b and 13.18b), a raised contour map, a shaded relief map, and so on. The present section is not concerned with the graphic representation of maps, but instead with the ways mapped values are obtained. Spatial interpolation methods have been reviewed by Lam (1983).

Geographic information systems (GIS) are widely used nowadays, especially by geographers and increasingly by ecologists, to manage complex data corresponding to points, lines, and surfaces in space. The present section is not an introduction to these complex systems. It only aims at presenting the most widespread methods for mapping univariate data (i.e. a single variable y). The spatial analysis of multivariate data (multivariate matrix **Y**) is deferred to Sections 13.3 to 13.5.

Beware of non-additive variables such as pH, logarithms of counts of organisms, diversity measures, and the like (Subsection 1.4.2). Maps of such variables, produced by trend-surface analysis or interpolation methods, should be interpreted with caution because the interpolated values of such variables only make sense by reference to sampling units of the same size as those used in the original sampling design. Block kriging (Subsection 13.2.2) for blocks representing surfaces or volumes that differ from the grain of the observed data does not make sense for non-additive variables.

1 — Trend-surface analysis

Trend-surface analysis is the oldest method for producing smoothed maps. In this method, estimates of the variable at given locations are not obtained by interpolation, as in the methods presented in Subsection 13.2.2, but through a regression model calibrated over the entire study area.

In 1914, W. S. Gosset, writing under the pseudonym Student, proposed to express observed values as a polynomial function of time and mentioned that it could be done for spatial data as well. This is also one of the most powerful tools of spatial pattern analysis, and certainly the easiest to use. The objective is to express a response variable y as a nonlinear function of the geographic coordinates X and Y of the sampling sites where the variable was observed:

$$y = f(\mathrm{X}, \mathrm{Y})$$

In many cases, a polynomial of X and Y with cross-product terms is used; trend-surface analysis is then an application of polynomial regression (Subsection 10.3.4) to spatially-distributed data. For example a relatively complex, but smooth surface might be fitted to a variable using a third-order polynomial with 10 parameters (b_0 to b_9):

$$\hat{y} = f(\mathrm{X}, \mathrm{Y}) = b_0 + b_1\mathrm{X} + b_2\mathrm{Y} + b_3\mathrm{X}^2 + b_4\mathrm{XY} + b_5\mathrm{Y}^2 + b_6\mathrm{X}^3 + b_7\mathrm{X}^2\mathrm{Y} + b_8\mathrm{XY}^2 + b_9\mathrm{Y}^3 \quad \textbf{(13.19)}$$

Note the distinction between the response variable y, which may represent a physical or biological variable, and the Cartesian geographic coordinate Y. Using polynomial regression, trend-surface analysis produces an equation that is linear in its parameters, although the response of y to the explanatory variables in matrix $\mathbf{X} = [\mathrm{X,Y}]$ may be nonlinear. If variables y, X and Y have been centred on their respective means prior to model fitting, the model has an intercept of 0 by construct; hence parameter b_0 does not have to be fitted and it can be removed from the model.

Numerical example. The data from Table 10.6 are used here to illustrate the method of trend-surface analysis. The dependent variable of the analysis, y, is Ma, which was the log-transformed ($\log_e(x + 1)$) concentrations of aerobic heterotrophic bacteria growing on marine agar at salinity of 34 psu. The explanatory variables are the X and Y geographic coordinates of the sampling sites (Fig. 13.15a). The steps of the calculations are the following:

- Centre the geographic coordinates on their respective means. The reason for centring X and Y is given in Subsection 10.3.4; the amount of variation explained by a trend-surface equation is not changed by a translation (centring) of the spatial coordinates across the map.

- Determine the order of the polynomial equation to be used. A first-degree regression equation of Ma as a function of the geographic coordinates X and Y alone would only represent the linear variation of Ma with respect to X and Y; in other words, a flat surface, possibly sloping with respect to X, Y, or both. With the present data, the first-degree regression equation was not significant ($R^2 = 0.02$), meaning that there was no significant linear geographic trend to be described in the data. A regression equation incorporating the second-degree monomials (X^2, XY and Y^2) together with X and Y would be appropriate to model a surface presenting a single

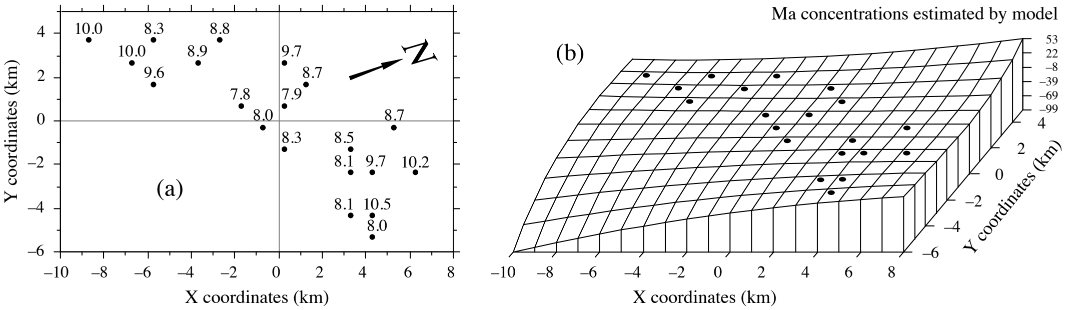

Figure 13.15 Variable Ma (log-transformed concentrations of aerobic heterotrophic bacteria growing on marine agar at salinity of 34 psu) at 20 sites in the Thau coastal lagoon, France, on 25 October 1988. (a) Map of the sampling sites with respect to arbitrary geographic coordinates X and Y. The observed values of Ma, from Table 10.6, are also shown. The *N* arrow points to the north. (b) Trend-surface map; the vertical axis gives the values of Ma estimated by the polynomial regression equation. Dots represent the sampling sites.

large bump or trough. Again, this did not seem to be the case with the present data since the second-degree equation was not significant ($R^2 = 0.39$). An equation incorporating the third-degree, fourth-degree, etc. terms would be able to model structures of increasing complexity and refinement. The cost, however, is a loss of degrees of freedom for every new monomial in the equation; trend-surface analysis using high-order equations thus requires a large number of observed sampling sites. In the present example, the polynomial was limited to the third degree, for a total of 9 terms; this is a large number of terms, considering that the data only contained 20 sampling sites.

• Using the values of coordinates X and Y, calculate the terms of the third-degree polynomial, by combining variables X and Y as follows: X^2, X×Y, Y^2, X^3, X^2×Y, X×Y^2, Y^3. Alternatively, one could compute a third degree orthogonal polynomial of the geographic coordinates. Ordinary and orthogonal polynomials can both be computed by function ***poly()*** in R (Section 13.6).

• Compute the multiple regression equation. The model obtained using all 9 regressors had $R^2 = 0.87$, but several of the partial regression coefficients were not significant.

• Remove nonsignificant terms. The linear terms may be important to express a linear gradient; the quadratic and cubic terms may be important to model more complex surfaces. Nonsignificant terms should not be left in the model, except when they are required for comparison purpose. Nonsignificant terms were removed one by one (backward elimination, Subsection 10.3.3) until all terms (monomials) in the polynomial equation were significant. The resulting trend-surface equation was highly significant ($R^2 = 0.81$, $p < 0.0001$):

$$\hat{y} = 8.13 - 0.16\,XY - 0.09\,Y^2 + 0.04\,X^2Y + 0.14\,XY^2 + 0.10\,Y^3$$

Remember, however, that tests of significance are too liberal with autocorrelated data, due to the non-independence of residuals, with the consequence that nonsignificant relationships are declared significant too often (Subsection 1.1.2).

- Lay out a regular grid of points (X', Y') and, using the regression equation, compute forecasted values ($\hat{y}'$) for these points. Plot a map (Fig. 13.15b) using the file with (X', Y', and $\hat{y}'$). Values estimated by a trend-surface equation at the study sites do not coincide with the values observed at these sites; regression is not an exact interpolator, contrary to kriging (Subsection 13.2.2).

Different features could be displayed by rotating the figure. The orientation chosen in Fig. 13.15b does not clearly show that the values along the long axis of the Thau lagoon are smaller near the centre than at the ends. It displays, however, the wavy structure of the data from the lower left-hand to the upper right-hand corner, which is roughly the south-to-north direction. The figure also clearly indicates that one should refrain from interpreting extrapolated data values, i.e. values located outside the area that has actually been sampled. In the present example, the values forecasted by the model in the lower left-hand and the upper right-hand corners (–99 and +53, respectively) are meaningless for log bacterial concentrations. Within the area where real data are available, however, the trend-surface model provides a good visual representation of the broad-scale spatial variation of the response variable.

Examination of the residuals is essential to make sure that the model is not missing some salient feature of the data. If the trend-surface model has extracted all the spatially-structured variation of the data, given the scale of the study, residuals should look random when plotted on a map and a correlogram of residuals should be non-significant. With the present data, residuals were small and did not display any recognizable spatial pattern.

A cubic trend-surface model is often appropriate with ecological data. Consider an ecological phenomenon that starts at the mean value of the response variable y at the left-hand border of the sampled area, increases to a maximum, then goes down to a minimum, and comes back to the mean value at the right-hand border. The amount of space required for the phenomenon to complete a full cycle — whatever the shape it may take — is its extent (Section 13.0). Using trend-surface analysis, such a phenomenon would be correctly modelled by a third-degree trend surface equation.

The degree of the polynomial that is appropriate to model a phenomenon is partly predictable. If the extent is of the same order as the size of the study area (say, in the X direction), the phenomenon will be correctly modelled by a polynomial of degree 3, which has two extreme values, a minimum and a maximum. If the extent is larger than the study area, a polynomial of degree less than 3 is sufficient; degree 2 if there is only one maximum, or one minimum, in the sampling window; and degree 1 if the study area is limited to the increasing, or decreasing, portion of the phenomenon. Conversely, if the scale of the phenomenon controlling the variable is smaller than the study area, more than two extreme values (minima and maxima) will be found, and a polynomial of order larger than 3 is required to model it correctly. The same reasoning applies to the X and Y directions when using a polynomial combining the X and Y geographic coordinates. So, using a polynomial of degree 3 acts as a filter: it is a way of looking for phenomena that are of the same extent, or larger, than the study area.

An assumption must be made when using the method of trend-surface analysis: that all observations form a single statistical population, subjected to one and the same generating process, and can consequently be modelled using a single polynomial equation of the geographic coordinates. Evidence to that effect may be available prior to the analysis. When that is not the case, the hypothesis of homogeneity may be supported by examining the regression residuals (Subsection 10.3.1). When there are indications that values in different regions of the geographic space obey different processes (e.g. different geology, action of currents or wind, or influence of other physical variables), the study area should be divided into regions, to be modelled by separate trend-surface equations.

Polynomial regression, as used in the numerical example above, is a good first approach to fitting a model to a surface when the shape to be modelled is unknown, or known to be simple. In some instances, however, it may not provide a good fit to the data; trend-surface analysis must then be conducted using nonlinear regression (Subsection 10.3.6), which requires that an appropriate numerical model be provided to the estimation program. Consider the example of the effect of some human-generated environmental disturbance at a site, the indicator variable being the number of species. The response, in that case, is expected to be stronger near the impacted site, tapering off as one gets farther away from it.

Assuming that data were collected along a transect (a single geographic coordinate X) and that the impacted site was near the centre of the transect, a polynomial equation would not be appropriate to model an inverse-squared-distance diffusion process (Fig. 13.16a). An equation of the form:

$$\hat{y} = b_0 + \frac{b_1 \mathrm{X}^2}{b_2 \mathrm{X}^2 + 1}$$

would provide a much better fit (Fig. 13.16b). The minimum of that equation is b_0; this value occurs when $\mathrm{X} = 0$. The maximum, b_1/b_2, is reached asymptotically as X becomes large in either the positive or negative direction. For data collected in different directions around the impacted site, a nonlinear trend-surface equation with similar properties would be of the form:

$$\hat{y} = b_0 + \frac{b_1 \mathrm{X}^2 + b_2 \mathrm{Y}^2}{b_3 \mathrm{X}^2 + b_4 \mathrm{Y}^2 + 1}$$

where X and Y are the coordinates of the sites in geographic space.

Trend-surface analysis is appropriate for describing broad-scale spatial trends in data, but it does not produce accurate fine-grained maps of the spatial variation of a variable. Other methods described in Chapter 14 allow researchers to model variation at finer scales. In some studies, the broad-scale trend itself is of interest; this is the case in the numerical example above and in Ecological application 13.2. In other situations, and especially in studies that cover large geographic expanses, the broad-scale trend may be already known and understood; researchers interested in geographic variation patterns may want to conduct analyses on detrended data, i.e. data from which the Detrending

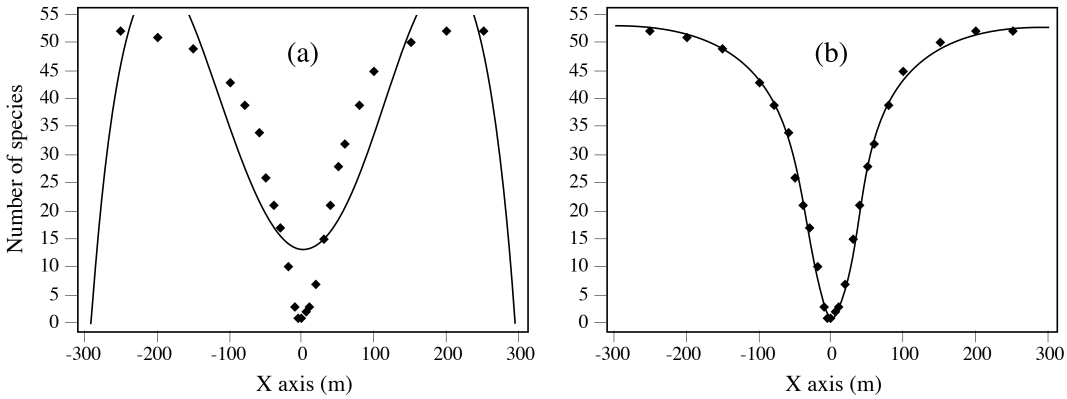

Figure 13.16 (a) Artificial data representing the number of species around the site of an environmental disturbance (located at X = 0) are not well-fitted by a 4th-order polynomial equation of the X coordinates ($R^2 = 0.7801$). (b) They are well-fitted by the following inverse-squared-distance diffusion equation: $\hat{y} = 1 + [0.0213X^2 / (0.0004X^2 + 1)]$ ($R^2 = 0.9975$).

broad-scale trend has been removed. Detrending a variable may be achieved by computing the residuals from a trend-surface equation of sufficient order, as in time-series analysis (Section 12.2).

If there is replication at each geographical observation point, it is possible to perform a test of goodness-of-fit of a trend-surface model (Draper and Smith, 1981; Legendre & McArdle, 1997). By comparing the observed error mean square after fitting the trend surface to the error mean square estimated by the among-replicate within-location variation, one can test if the model fits the data properly. The latter variation is computed from the deviations from the means at the various locations; it is the residual mean square of an ANOVA testing for differences among locations. When the trend surface goes through the expected values at the various locations, these two error mean squares are not much different, and their F-ratio does not significantly differ from 1. If, on the contrary, the fitted surface does not follow the major features of the variation among locations, the deviations of the data from the fitted trend-surface values are larger than the residual within-location variation. The F-statistic is then significantly larger than 1, indicating that the trend surface is misrepresenting the variation among locations.

Numerical example. Consider the artificial data in Fig. 13.17. Variable X represents a geographic axis along which sampling has taken place at 6 sites with replication. Variable y was constructed using equation $y = 2.5X - 0.3X^2 + \varepsilon$, where ε is a random standard normal deviate [N(0,1)]. A quadratic trend-surface model of X was fitted to the data. The residual mean square, or "error mean square after fitting the trend surface", was $MS_1 = 0.84909$ ($\nu = 27$). An analysis of variance was conducted on y using the grouping of data into 6 sites as the classification

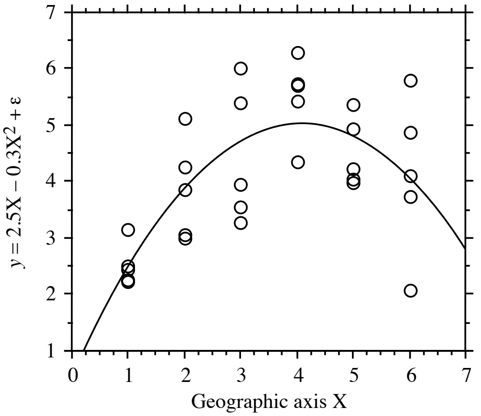

Figure 13.17 Artificial data representing sampling along a geographic axis X with 5 replicates at each site; $n = 30$. The F-test of goodness-of-fit indicates that the trend-surface equation $\hat{y} = 0.562 + 2.184X - 0.267X^2$ ($R^2 = 0.4899$) fits the data properly.

criterion. The residual mean square obtained from the ANOVA was $MS_2 = 0.87199$ ($\nu = 24$). The ratio of these two mean squares gave an F-statistic:

$$F = \frac{MS_1}{MS_2} = \frac{0.84909}{0.87199} = 0.97374$$

which was tested against $F_{\alpha=0.05(27,\,24)} = 1.959$. The F-statistic was not significantly different from 1 ($p = 0.530$), which indicated that the model fitted the data properly.

The trend-surface analysis was recomputed using a linear model of X. The model obtained was $\hat{y} = 3.052 + 0.316X$ ($R^2 = 0.1941$). MS_1 in this case was 1.29358 ($\nu = 28$). The F-ratio $MS_1/MS_2 = 1.29358/0.87199 = 1.48348$. The reference value was $F_{0.05(28,\,24)} = 1.952$. The probability associated with the F-ratio, $p = 0.165$, indicated that this model still fitted the data, which were constructed to contain a linear term (2.5X in the construction equation) as well as a quadratic trend (term $-0.3X^2$), but the fit was poorer than with the quadratic polynomial model, which was capable of accounting for both the linear and quadratic trends.

This numerical example shows that trend-surface analysis may be applied to data collected along a transect; the "trend surface" is one-dimensional in that case. The numerical example at the end of Subsection 10.3.4 is another example of a trend-surface analysis of a dependent variable, salinity, with respect to a single geographic axis (Fig. 10.9). Trend-surface analysis may also be used to model data in three-dimensional geographic space (geographic coordinates X, Y and Z, where Z is either altitude or depth), or with one of the dimensions representing time. Section 13.5 will show how the analysis may be extended to a multivariate dependent data matrix **Y**.

(a)

35	41	37	48	52	68	64	51	52	19	50	48	46	50	40	33	27	29	32	39
22	47	46	33	51	71	54	71	44	56	63	50	30	49	46	41	43	40	29	32
45	66	58	60	27	59	50	52	41	40	54	39	41	46	47	19	24	30	20	28
41	56	33	60	59	60	53	52	26	39	31	33	29	54	37	18	36	42	27	29
48	36	38	34	41	55	42	67	53	57	34	34	42	33	32	46	33	18	27	32
41	32	41	35	48	52	40	56	40	44	41	43	44	41	43	32	22	34	30	32
17	29	50	67	35	52	28	44	45	28	30	35	30	28	35	37	20	28	50	31
27	43	38	44	29	44	35	39	44	38	40	24	37	43	35	31	38	48	50	37
27	42	36	36	29	46	39	38	29	37	38	35	35	38	25	38	39	54	50	44
52	41	32	41	42	28	47	22	24	17	37	31	38	29	41	38	36	46	38	52

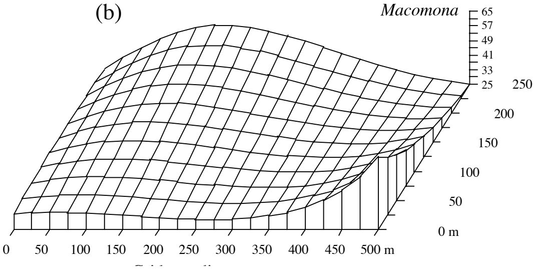

Figure 13.18 *Macomona* > 15 mm at 200 sites in Manukau Harbour, New Zealand, on 22 January 1994. (a) Actual counts at sampling sites in 200 regular grid cells; in the field, sites were not perfectly equispaced. (b) Map of the trend-surface equation explaining 32% of the spatial variation in the data. The values estimated from the trend-surface equation (log-transformed data) were back-transformed to raw counts before plotting. Modified from Legendre *et al.* (1997).

Haining (1987) described alternative methods for estimating the parameters of a trend-surface model when the residuals are spatially autocorrelated; in that case, least-squares estimation of the parameters is inefficient and standard errors as well as tests of significance are biased. Haining's methods allow one to recognize three components of spatial variation corresponding to the site, local, and regional scales, respectively.

Ecological application 13.2

A survey was conducted at 200 locations within a fairly homogeneous 12.5 ha rectangular sandflat area in Manukau Harbour, New Zealand, to identify factors that controlled the spatial distributions of the two dominant bivalves, *Macomona liliana* Iredale and *Austrovenus stutchburyi* (Gray), and to look for evidence of adult-juvenile interactions within and between species. Results were reported by Legendre *et al.* (1997). Most of the broad-scale spatial structure detected in the bivalve counts (two species, several size classes) was explained by the physical and biological variables. Results of principal component analysis and spatial regression modelling suggested that different factors controlled the spatial distributions of adults and juveniles. Larger size classes of both species displayed significant spatial structures, with physical variables explaining some but not all of this variation; the spatial patterns of the two species differed, though. Smaller organisms were less strongly spatially structured; virtually all of their spatial structure was explained by physical variables.

Highly significant trend-surface equations were found for all bivalve species and size classes (log-transformed data), indicating that the spatial distributions of the organisms were not random, but highly organised at the scale of the study site. The trend-surface models for smaller animals had much smaller coefficients of determination (R^2 = 0.10-0.20) than for larger animals (R^2 = 0.30-0.55). The best models, i.e. those with the highest R^2, were for the *Macomona* > 15 mm and *Austrovenus* > 10 mm. The coefficients of determination were consistently higher for *Austrovenus* than for *Macomona*, despite the fact that *Macomona* were usually far more

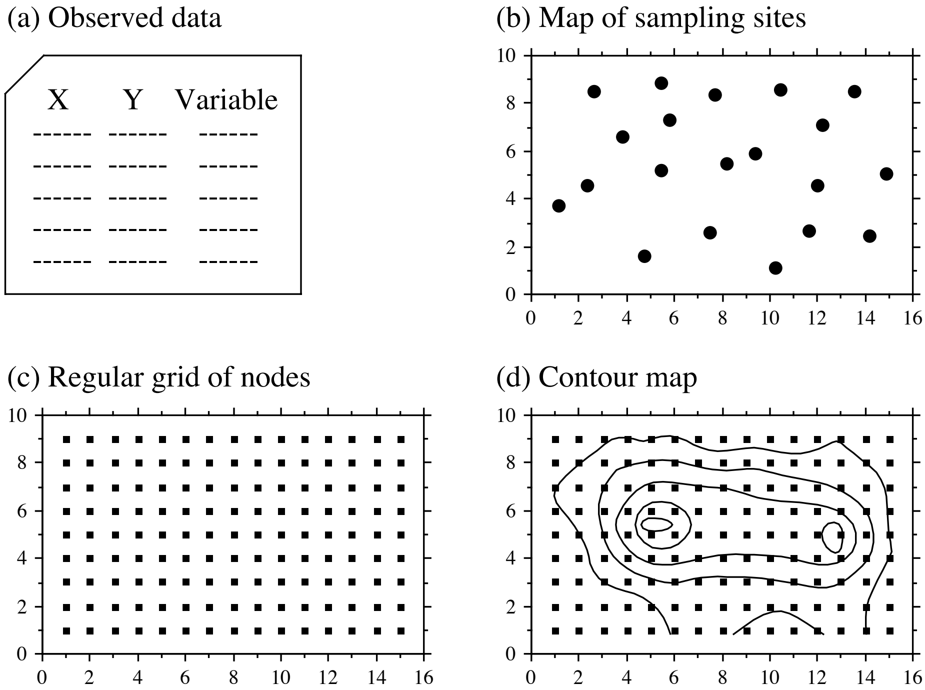

Figure 13.19 Summary of the interpolation procedure.

numerous than *Austrovenus*. A map illustrating the trend-surface equation is presented for the largest *Macomona* size class (Fig. 13.18); the field counts are also shown for comparison.

2 — Interpolated maps

In the family of interpolated map methods, the value of the variable at a point location on a map is estimated by local interpolation, using only the observations available in the vicinity of the point of interest. In this respect, interpolation mapping differs from trend surface analysis (Subsection 13.2.1), where estimates of the variable at given locations were not obtained by interpolation, as in the present subsection, but through a statistical model whose parameters were estimated from all observations in the study area. Figure 13.19 illustrates the principle of interpolation mapping. A regular grid of nodes (Fig. 13.19c) is defined over the area that contains the study sites $Ø_i$ (Fig. 13.19a, b). Interpolation assigns a value to each point of the grid. This is the single most important step in mapping. Following that, results may be represented in the form of contours (e.g. Fig. 13.19d) with or without colours or shades, or three-dimensional constructs such as Fig. 13.18b.

Figure 13.20 To estimate the value at a grid node (square), draw a search circle around it and consider the observed points ($Ø_i$) found within the circle. Observed points are separated from the node by distances $D(Ø_i$, Node).

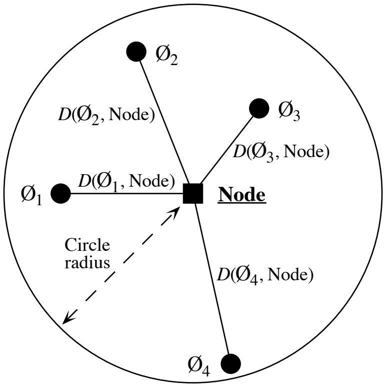

Estimating the value corresponding to each grid node may be done in different ways. Different interpolation methods may produce maps that look different; this is also the case when using different parameters with a same method (e.g. different exponents in inverse-distance weighting).

The most simple rule would be to give, to each node of the grid, the value of the observation which is the closest to it. The end result is a division of the map into Voronoï polygons (Subsection 13.3.1) displaying a "zone of influence" drawn around each observation. Another simple solution consists in dividing the map into Delaunay triangles (Subsection 13.3.1). There is an observed value y_i at each site $Ø_i$. A triangular portion of plane, adjusted to the points $Ø_i$ that form the vertices (corners) of a Delaunay triangle, provides interpolated values for all points inside the triangle. Maps obtained using these solutions are shown in Chapter 11 of Isaaks & Srivastava (1989).

Alternatively, one may draw a "search circle" (or an ellipsoid for anisotropic data) around each grid node (Fig. 13.20). The radius of the circle may be determined in either of two ways. (1) One may fix a minimum number of observed points that must be included in the interpolation for each grid node; or (2) one may use the "distance of influence of the process" found by correlogram or variogram analysis (Section 13.1). The estimation procedure is repeated for each node of the grid. Several methods of interpolation may be used.

- Mean. — Consider all the observed study sites found within the circle; assign the mean of these values to the grid node. This method does not produce smooth maps; discontinuities in neighbouring grid node values occur as observed points move in or out of the search circle.

• Inverse-distance weighting. — Consider the observation sites found within the circle and calculate a weighted mean value, using the formula:

$$\hat{y}_{\text{Node}} = \sum_i w_i y_i \qquad \textbf{(13.20)}$$

where y_i is the value observed at point Ø$_i$ and weight w_i is the inverse of the distance (D) from point Ø$_i$ to the grid node to be estimated. The inverse distances, to some power k, are scaled by the sum of the weights for all points Ø$_i$ in the estimation, so as to produce values that are consistent with the values observed at points Ø$_i$ (unbiasedness condition):

$$w_i = \left(\frac{1}{D(\text{Ø}_i, \text{Node})^k}\right) \Big/ \sum_i \frac{1}{D(\text{Ø}_i, \text{Node})^k} \qquad \textbf{(13.21)}$$

A commonly-used exponent is $k = 2$. This corresponds, for instance, to the decrease in energy of waves dispersing across a two-dimensional surface. The greater the value of k, the less influence distant data points have on the value assigned to the grid node. This method produces smooth values over the grid of nodes. The range of estimated values is smaller than the range of observed data so that, contrary to trend-surface analysis (Fig. 13.15b), inverse-distance weighting does not produce meaningless values in the parts of the map beyond the area that was actually sampled. When the observation sites Ø$_i$ do not form a regular or nearly regular grid, however, this interpolation method may generate features in maps that have little to do with reality. As a consequence, inverse-distance weighting is not recommended in that situation.

• Weighted polynomial fitting. — In this method, a trend-surface equation (Subsection 13.2.1) is adjusted to the observed data points within the search circle, weighting each observation Ø$_i$ by the inverse of its distance (using some appropriate power k) to the grid node to be estimated. A first or second-order polynomial equation is usually used. The value estimated by the polynomial equation for the coordinates of a grid node is denoted z_{Node}. This method suffers from the same problem as inverse distance weighting with respect to observation sites Ø$_i$ that do not form a regular or nearly regular grid of points.

Kriging

• Kriging. — This is the mapping tool in the toolbox of geostatisticians. The method was named by Matheron after the South African geostatistician D. G. Krige, who was the first to develop formal solutions to the problem of estimating ore reserves from sampling (core) data (Krige, 1952, 1966). Geostatistics was developed by Matheron (1962, 1965, 1970, 1971, 1973) and co-workers at the *Centre de morphologie mathématique* of the *École des Mines de Paris*. Geostatistics comprises the estimation of variograms (Subsection 13.1.3), kriging, validation methods for kriging estimates, and simulations methods for geographically distributed ("regionalized") data. Major textbooks have been written by former students of Matheron: David (1977) and Journel & Huijbregts (1978). Other useful references are Clark (1979), Rendu (1981), Verly *et al.* (1984), Armstrong (1989), Isaaks & Srivastava (1989), and Cressie (1991). Applications to environmental sciences and ecology have been discussed by Gilbert & Simpson (1985), Robertson (1987), Armstrong *et al.* (1989), Legendre & Fortin (1989), Soares *et al.* (1992), and Rossi *et al.* (1992). Geostatistical methods can be implemented using the software library of Deutsch & Journel (1992).

As in inverse-distance weighting (eq. 13.20), the estimated value for any grid node is computed as:

$$\hat{y}_{\text{Node}} = \sum_i w_i y_i$$

The chief difference between kriging and inverse-distance weighting is that, in kriging, the weights w_i applied to the points Ø$_{\text{i}}$ used in the estimation are not standardized inverses of the distances to some power *k*. Instead, the weights are based upon the covariances (semi-variances, eqs. 13.9 and 13.10) read on a variogram model (Subsection 13.1.3). They are found by linear estimation, using the equation:

$$\begin{array}{ccccc} \mathbf{C} & \cdot & \mathbf{w} & = & \mathbf{d} \\ \begin{bmatrix} c_{11} & \dots & c_{1n} & 1 \\ \cdot & \dots & \cdot & 1 \\ \cdot & \dots & \cdot & 1 \\ c_{n1} & \dots & c_{nn} & 1 \\ 1 & \dots & 1 & 0 \end{bmatrix} & & \begin{bmatrix} w_1 \\ \cdot \\ \cdot \\ w_n \\ \lambda \end{bmatrix} & = & \begin{bmatrix} d_1 \\ \cdot \\ \cdot \\ d_n \\ 1 \end{bmatrix} \end{array} \qquad \textbf{(13.22)}$$

where **C** is the covariance matrix among the *n* points Ø$_i$ used in the estimation, i.e. the semi-variances corresponding to the distances separating the various pair of points, provided by the variogram model; **w** is the vector of weights to be estimated (with the constraint that the sum of weights must be 1); and **d** is a vector containing the covariances between the various points Ø$_i$ and the grid node to be estimated. This is where a variogram model becomes essential; it provides the weighting function for the entire map and is used to construct matrix **C** and vector **d** for each grid node to be estimated. Element λ in vector **w** is a Lagrange parameter (as in Section 4.4) introduced to minimize the variance of the estimates under the constraint $\Sigma w_i = 1$ (unbiasedness condition). The solution to this linear system is obtained by matrix inversion (Section 2.8):

$$\mathbf{w} = \mathbf{C}^{-1}\,\mathbf{d} \qquad \textbf{(13.23)}$$

Vector **d** plays a role similar to the weights in inverse-distance weighting since the covariances in vector **d** decrease with distance. Using covariances, the weights are statistical in nature instead of geometrical.

Kriging takes into account the grouping of observed points $Ø_i$ on the map. When two points $Ø_i$ are close to each other, the value of the corresponding coefficient c_{ij} in matrix **C** is high; this contributes to lowering their respective weights w_i. In this way, the redundancy of information introduced by dense groups of sampling sites is taken into account.

When anisotropy is present, kriging can use two, four, or more variogram models computed for different geographic directions and combine their estimates when calculating the covariances in matrix **C** and vector **d**. In the same way, when estimation is performed for sampling sites in a volume, a separate variogram can be used to describe the vertical spatial variation. Kriging is the best interpolation method for data that are not on a regular grid or display anisotropy. The price to pay is increased mathematical complexity during interpolation.

Among the interpolation methods, kriging is the only one that provides a measure of the error variance for each value estimated at a grid node. For each grid node, the error variance, called *ordinary kriging variance* (s_{OK}^2), is calculated as follows (Isaaks & Srivastava, 1989), using vectors **w** and **d** from eq. 13.22:

$$s_{\mathrm{OK}}^2 = \mathrm{Var}[y_i] - \mathbf{w}'\mathbf{d} \qquad \textbf{(13.24)}$$

where $\mathrm{Var}[y_i]$ is the maximum-likelihood estimate of the variance of the observed values y_i (eq. 13.15). Equation 13.24 shows that s_{OK}^2 only depends on the variogram model and the local density of points, and not on the values observed at points $Ø_i$. The ordinary kriging variance may be used to construct confidence intervals around the grid node estimates at some significance level α, using eq. 13.4. It may also be mapped directly. Regions of the map with large values s_{OK}^2 indicate that more observations should be made because sampling intensity was too low.

Kriging, as described above, provides point estimates at grid nodes. Each estimate actually applies to a “point” whose size is the same as the grain of the observed data. The geostatistical literature also describes how *block kriging* may be used to obtain estimates for blocks (i.e. surfaces or volumes) of various sizes. Blocks may be small, or a single block may cover the whole map if one wishes to estimate a resource over a whole area. As mentioned in the introductory remarks of the present section, only additive variables can be used in block kriging. Block kriging programs always assume that the variable is *intensive*, e.g. concentration of organisms (Subsection 1.4.2). For *extensive* variables, such as the number of individual trees, one must multiply the block estimate by the ratio (block size / grain size of the original data).

3 — Measures of fit

Different measures of fit may be used to determine how well an interpolated map represents the observed data. With most methods, some measure may be constructed of the closeness of the estimated (i.e. interpolated) values $\hat{y}_i$ to the values y_i observed at sites Ø$_i$. Four easy-to-use measures are:

- The mean absolute error: $MAE = \frac{1}{n}\sum_i |y_i - \hat{y}_i|$;

- The mean squared error: $MSE = \frac{1}{n}\sum_i (y_i - \hat{y}_i)^2$;

- The Euclidean distance: $D_1 = \sqrt{\sum_i (y_i - \hat{y}_i)^2}$;

- The correlation coefficient (r) between values y_i and $\hat{y}_i$ (eq. 4.7). In the case of a trend-surface model, the square of this correlation coefficient is the coefficient of determination of the model.

In the case of kriging, the above measures of fit cannot be used because the estimated and observed values are equal at all observed sites Ø$_i$. The technique of cross-validation can be used instead (Isaaks & Srivastava, 1989, their Chapter 15). One observation, say Ø$_1$, is removed from the data set and its value is estimated using the remaining points Ø$_2$ to Ø$_n$. The procedure is repeated for Ø$_2$, Ø$_3$, …, Ø$_n$. One of the measures of fit described above may be used to measure the closeness of the estimated to the observed values. If replicated observations are available at each sampling site (a situation that does not often occur), the F-test of goodness-of-fit described in Subsection 13.2.1 can be used with all interpolation methods.

13.3 Patches and boundaries

Multivariate data may be condensed into spatially-constrained clusters. These may be displayed on maps, using different colours or shades. The present section explains how clustering algorithms can be constrained to produce groups of spatially contiguous sites; study of the boundaries between homogeneous zones is also discussed. Prior to clustering, one must state unambiguously which sites are neighbours in space; the most common solutions to this problem are presented in Subsection 13.3.1.

1 — Connection networks

When sampling has been conducted on a regular rectangular grid, neighbouring points may be linked using simple connecting schemes whose names are derived from the game of chess (Cliff & Ord, 1981): rook's (rectangular: Fig. 13.21a), bishop's (diagonal: Fig. 13.21b), or king's connections (also called queen's: both rectangular and diagonal, Fig. 13.21c). Sampling in staggered rows leads to connecting each point